



# Review of improvement of machinability and surface integrity in machining on aluminum alloys

Danil Yu Pimenov<sup>1</sup> · Maitri Kiran<sup>2</sup> · Navneet Khanna<sup>2</sup> · Giuseppe Pintaude<sup>3</sup> · Marina Cardozo Vasco<sup>3</sup> · Leonardo Rosa Ribeiro da Silva<sup>4</sup> · Khaled Giasin<sup>5</sup>

Received: 5 June 2023 / Accepted: 30 October 2023 / Published online: 14 November 2023  
© The Author(s) 2023

## Abstract

Aluminum alloys are widely used in many industries, including aerospace, automotive, civil, and electrical engineering. When compared to pure aluminum, most aluminum alloys have lower electrical and thermal conductivity, corrosion resistance, and weldability, as well as a low density and specific gravity. At the same time, the properties of aluminum alloys vary significantly depending on the group, which has a significant impact on their machinability. This review article is focused on the study of machining characteristics of aluminum alloys, such as machinability, surface integrity, tool wear and tool life, material removal rate (MRR), and chip morphology. The directions of increasing machinability by controlling cutting parameters, cutting environment, such as dry machining, conventional cooling systems, minimum quantity of lubricant (MQL), cryogenic lubrication (CL), with tool geometry, and textured tools, are also considered; tool materials include coating, vibration, thermally, and hybrid assisted machining. The article discusses the main types of machining, namely, turning, milling, drilling, and grinding. It shows ways to increase the machinability of machining on aluminum alloys, as well as the advantages and disadvantages. From the literature, it can be concluded that tool wear when machining aluminum alloys is 30–40% lower than when machining steel alloys due to their higher ductility and lower strength. Surface integrity, affected by the cutting parameters and cutting temperatures — which can reach between 200 and 400 °C — can vary by up to 15% in hardness and 20% in surface roughness. Cutting tool characteristics can enhance surface finish by up to 25% and extend tool life, reducing edge formation by up to 30%. Chip morphology, influenced by factors such as cutting parameters and tool material, can improve tool life by up to 35%. Vibration techniques can reduce thermal effects and improve surface finish by up to 40%, reducing cutting forces by around 30%.

**Keywords** Aluminum alloys · Machining · Surface integrity · Machinability · Tool wear · Chip morphology

---

✉ Danil Yu Pimenov  
danil\_u@rambler.ru

✉ Navneet Khanna  
navneetkhanna@iitram.ac.in

✉ Khaled Giasin  
Khaled.giasin@port.ac.uk

Maitri Kiran  
maitri.kiran.19e@iitram.ac.in

Giuseppe Pintaude  
pintaude@utfpr.edu.br

Marina Cardozo Vasco  
marina.mcv@gmail.com

Leonardo Rosa Ribeiro da Silva  
leorrs@ufu.br

<sup>1</sup> Department of Automated Mechanical Engineering, South Ural State University, Lenin Prosp. 76, Chelyabinsk 454080, Russia

<sup>2</sup> Advanced Manufacturing Laboratory, Institute of Infrastructure Technology, Research and Management, Ahmedabad 380008, India

<sup>3</sup> Academic Department of Mechanics, Universidade Tecnológica Federal Do Paraná, Curitiba, Brazil

<sup>4</sup> School of Mechanical Engineering, Federal University of Uberlândia, Av. João Naves de Ávila, Bloco 1M, Uberlândia, MG 212138400-902, Brazil

<sup>5</sup> School of Mechanical and Design Engineering, University of Portsmouth, Portsmouth PO1 3DJ, UK

## 1 Introduction

Aluminum is a soft and ductile metal that generally lends itself well to machining. In this case, the cutting conditions can be much higher than when machining, for example, structural steels [1]. On the one hand, this is due to lower loads during chip removal, on the other hand, the high thermal conductivity of aluminum, due to which heat is well removed from the cutting zone along with the chips, without causing overheating of the tool [2]. Sometimes when processing aluminum and alloys, negative effects can also be encountered. First, the high toughness of some alloys often leads to the formation of long chips, which wind around the tool and clog the grooves [3]. Secondly, in built-up edge formation, there is a spot welding of the material being processed on the cutting edge of the tool in the cutting zone, which can lead to an increase in the load on the tool, as well as the difficulty of chip flow [3]. The degree and depth of surfacing of the material is affected by cutting conditions, the geometry of the cutting tool, and the degree of its blunting; that is, all factors determine the flow of plastic deformation in the cutting zone.

Machinability is not a material property that can be defined by a single characteristic parameter. It is a complex technological term. Machinability depends both on the physical and chemical properties of the aluminum or aluminum alloy and on the manufacturing process that was used in the manufacture of the aluminum semi-finished product or product. However, from the type of alloy, from its physical and chemical properties, the machinability characteristic will change [4]. From the point of view of machinability, aluminum alloys are divided into the following groups (in order of increasing difficulty of machining): wrought aluminum alloys with low strength, wrought aluminum alloys with increased strength, aluminum alloys for machining, aluminum–silicon alloys with a silicon content of up to 10%, eutectic aluminum–silicon alloys, and hypereutectic aluminum–silicon alloys. Machinability includes such machining criteria as chip shape, cutting force, cutting tool wear, and surface quality after machining [5]. Comparative analysis of machinability of aluminum alloys in relation to other structural materials. Due to the low cutting forces during processing, aluminum and its alloys are easier to cut than steel or bronze [6]. This means that aluminum and its alloys can be machined faster than these materials.

Considering review articles aimed at researching machining processes for aluminum alloys, Bork et al. [7] reviewed information on the requirements, limitations, and machinability criteria for cutting fluids in high feed milling of 7050-T7451 aluminum alloy. Santos et al. [3] attempted to summarize the machinability characteristics

of aluminum alloys by summarizing the problems and some ways to solve these problems. Li and Wang [8] in a review showed a comprehensive view of the problems associated with residual stresses and distortions during the machining of aircraft-grade aluminum alloy parts. Del Sol et al. [9] in their work showed the current state of machining on thin-walled light alloys, with the analysis of different types of thin-walled parts, identifying the causes of instability and deformation using analytical models. In a previously published review [10], the drilling forces and parameters, geometry, materials, coatings of drills, chip shape, analysis of tool wear, and precision indicators such as hole size and roundness error, surface roughness, and burr formation were considered mainly for drilling Al2024 and Al7075 aluminum alloys. In Duan et al.'s review [2], for different conditions of the milling process of aluminum alloy, the cutting force models for the empirical model, the finite element model, and the model of the instantaneous milling force were shown. In their review, Sarikaya et al. [11] cooling methods are shown as of minimum quantity lubrication (MQL), nano-fluids-MQL, Ranque-Hilsch vortex tube MQL (RHVT + MQL), and cryogenic-MQL as alternative to flood cooling, aimed at increasing machinability and sustainability for light alloys. Kui et al. [1] discuss the use of a minimum amount of lubricant (MQL) when machining of steels, aluminum, and titanium alloys. It should be noted that there are very few reviews devoted to the machining of aluminum alloys. The emergence of aluminum alloys obtained with cryogenic treatment as shown in the review by Vijay et al. [12] have new properties and require special methods to improve machinability. In this case, most often they cover only a separate area of application of machining methods. And most importantly, there are no reviews that could give current modern methods aimed at improving the machinability and surface integrity in the machining of aluminum alloys. Thus, this review aims to overcome this shortcoming.

This review comprehensively discusses best practices for improving machinability and surface integrity in aluminum alloy machining operations such as turning, milling, drilling, and grinding. The article examined the improvement of machinability, taking into account the influence of cutting conditions, cutting environment (dry, conventional cooling system, minimum quantity lubrication (MQL), cryogenic lubrication (CL)), geometries, material, coating and textures of tools, vibration, and thermal and hybrid processing. Important aspects such as surface integrity, tool wear and tool life, material removal rate (MRR), and chip morphology are considered here. The structure of the article is as follows: Sect. 2 contains the classification and properties of aluminum alloys. Section 3 presents the machining parameters of aluminum alloys. Section 4 describes the methods for improving the machinability and surface integrity of

aluminum alloys in various aspects. Section 5 describes the challenges and future trends, while Sect. 6 presents the conclusions.

## 2 Aluminum alloys: classification and mechanical properties

### 2.1 Introduction

After steel, aluminum is the most highly produced metal and the most produced non-ferrous metal [13, 14], being produced in a higher volume than all other non-ferrous metals combined [15, 16]. In 2019, aluminum production surpassed 17.2 million tons, while copper, the second most produced non-ferrous material, reached 1.9 million tons and other non-ferrous metals combined summed up 2.1 million tons produced [16]. Primary aluminum production in the same year was of over 63.6 tons globally, according to the International Aluminum Institute [17]. Aluminum is being used to replace steel components, particularly in the aero-space and automotive industries. For each kilogram of aluminum that replaces ferrous alloys one can avoid up to 20 kg of GHG emissions [18]. Combining mechanical properties and corrosion resistance for aluminum alloys is usually achieved using some strategies. The most significant are the isothermal ageing, the multi-stage ageing, the non-isothermal ageing, the retrogression and re-ageing (RRA), and stress ageing (i.e., creep ageing) [19]. A general classification of aluminum alloys can be described in terms of the main route of fabrication: (i) casting alloys; (ii) work-hardening alloys; and (iii) age-hardening alloys [20]. The designation of aluminum alloys is usually made by a four-digit numerical system, for both wrought and cast alloys. However, for casting a decimal point is incorporated to identify alloys in the form of castings and foundry ingots [20]. Additional digits are used to designate the temper, in which 10 variations (T1 to T10) are described in detail by Rambabu et al. [20].

#### 2.1.1 Casting alloys

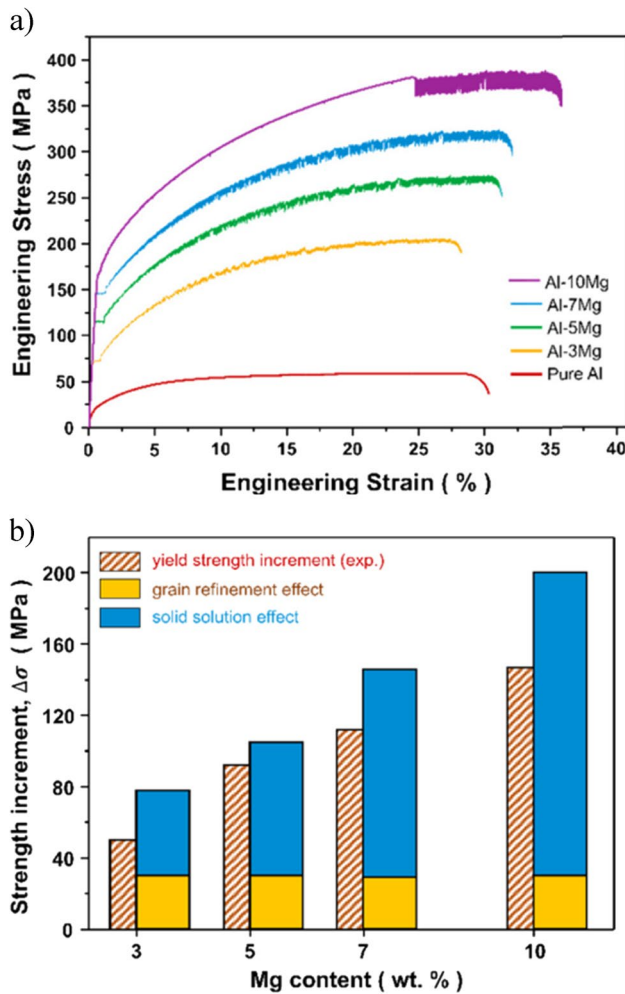
Casting aluminum alloys can be based on the eutectic reaction found at 12.6 wt% silicon. Javidani and Larouche [21] revised the applications of Al–Si alloys for engine components, indicating that hypoeutectic alloys 319 and 356+0.5Cu are the preferable for engine heads and engine blocks, followed by 390 alloy (hypereutectic). A better combination of tensile strength and ductility could be achieved by using severe plastic deformation methods, which refine grain size and diminish the impact of coarse Si particles, inherent to the increase of Si amount [22]. In the work performed by Umezawa and Nagai, the tensile strength of cold-worked materials ranged from 250 to 290 MPa, approximately twice

the values shown by the cast material [22]. Alloys based on the Al–Cu–Si system are lightweight and superior to Al–Si alloys in terms of strength and to Al–Cu alloys in terms of corrosion resistance [23, 24]. It is remarkable that these alloys have high concentrations of solutes, and to manufacture Al–Cu–Si alloys to meet certain requirements, it is essential to establish correlations of the phases characterizing the microstructures with thermal solidification parameters [25]. Silicon is mainly released in the form of primary precipitates and as an  $Al_9Fe_2Si_2$  compound in phases with aluminum and iron in amounts depending on the other constituents [26]. Awe [27] demonstrated that the Al–27 wt% Cu–5 wt% Si cast alloy displayed a high hardness of 224 HV as compared to the A319 alloy. In a different work, Awe [28] studied the microstructure and properties of the same Al–Cu–Si alloy rapidly solidified (immediately quenched in an ice-water mixture) and slowly solidified (cooled slowly in still air), with steel tubes as enclosed molds. The rapidly cooled samples showed a binary eutectic with an average spacing of 1.8  $\mu\text{m}$  and a ternary eutectic characterized by a spacing of 600 nm. The increased hardness of about 220 HV of the rapidly solidified alloy specimens was attributed to the homogeneous dispersion of fine Si particles in the eutectic matrix. In terms of machinability, Balos et al. [29] compared two casting alloys, ASC91 (9 wt% Si + 1 wt% Cu, 246-MPa ultimate tensile strength (UTS)) and ASC73 (7 wt% Si + 3 wt% Cu, 162-MPa UTS), tested under vertical milling machine. They concluded that the ASC73 alloy, with larger additions of copper, is preferable for cylinder head than the ASC91 alloy, considering its performance in terms of fatigue and machinability.

#### 2.1.2 Work hardening alloys

Al–Mg alloys, including the 5000 series of wrought alloys, and the 500 series of cast alloys [30] are known to have the highest strengths of all Al alloys without heat treatment, along with good corrosion resistance and weldability. Figure 1(a) shows the stress–strain curves of the rolled and annealed Al–Mg sheets containing different amounts of Mg compared to pure Al, while Fig. 1(b) shows the increase of strength of Al–Mg alloys with varying Mg content (3 to 10% wt) and grain refinement [31].

Although Fig. 1 shows that the solid solution effect is more effective than the grain refinement one, for casting alloys this strategy is very relevant to improve the as-cast properties [32, 33], since a finer grain size promotes good interdendritic feeding, reducing the number of casting defects, including porosity, macro-segregation, non-uniform properties, and hot and cold tearing [34, 35]. Darling et al. [36] achieved hardness of  $\sim 4$  GPa for Al–Mn alloys (2000 series), prepared high-energy mechanical alloying, which can be used to surpass the low solubility limit of Mn in

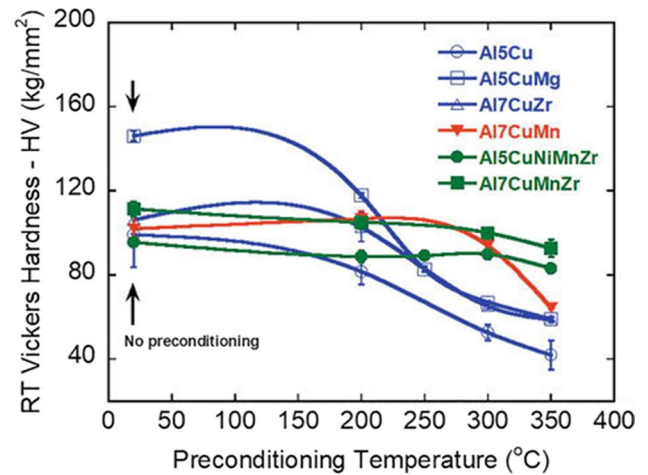


**Fig. 1** **a** Engineering stress–strain curves, as recorded during the tensile testing of the Al–xMg alloy sheets prepared by rolling and subsequent annealing. **b** Increase in the strength of the Al–xMg alloys resulting because of grain refinement (in yellow) and solution effects (in blue) [31]

nano-crystalline Al alloys. They concluded that the main strengthening mechanism was related to decreasing the grain size of the matrix.

### 2.1.3 Age-hardening alloys

Due to the excellent structural properties, such as low density, high fracture toughness, and fatigue strength, Al–Cu alloys (2000 series) are usually chosen to manufacture high-performance components, such as pressure vessels, liquid hydrogen tanks, and rocket engine fuel tanks [37, 38]. However, these alloys commonly present a relatively high coefficient of thermal expansion and low microyield strength, which may lead to dimensional instability when the material is in an alternating temperature field [38]. To ensure that the advantageous properties of these alloys will not be surpassed



**Fig. 2** Variation of hardness for various aluminum alloys combined with Cu, Mg, Zr, and Mn as a function of pre-conditioning temperatures [42]

by its drawbacks, different processes can be employed, such as precipitation hardening and artificial aging treatments [39], squeeze casting [40], and most recently, the precipitation of solute clusters by re-aging the material at high temperatures (420 °C) for extended periods of time (100 h) [41]. These treatments aim to increase the tensile strength and yield strength of Al–Cu alloys with minimum plasticity reduction.

Moreover, the addition of other alloying elements, such as Mn and Zr, also works for improving the benefits of heat treatments. Roy and Roy [42] showed that the ultimate tensile strength (UTS) of Al–5Cu alloy is ~490 MPa whereas it is ~300 MPa for Al–Cu–Mn–Zr alloy at room temperature (RT). However, after prolonged thermal exposure at 300 °C, the trend reverses; Al–Cu–Mn–Zr alloy possesses nearly twice the UTS compared to the base Al–Cu alloy. Similarly, an Al–5Cu–Mg alloy possesses higher hardness than Al–Cu–Mn–Zr alloys at RT, as shown in Fig. 2. Increasing pre-conditioning temperatures (heat treatment for 200 h), only Al–Cu–Mn–Zr alloys can sustain the room temperature hardness without any significant degradation until 350 °C.

The selection of suitable alloy elements allows aluminum alloys to keep their mechanical behavior at high temperatures. Aging hardening Al–Zn–Mg alloys (7000 series) can be considered as one of preferential chemical composition combinations for achieving excellent mechanical properties and good corrosion resistance [43, 44]. Increasing Mg content can lead to higher hardness and strength; however, in the presence of copper as an alloying element, the conductivity is reduced in a constant content of zinc (8.5 wt%). At the same time, this increasing in Mg content can result in intergranular fracture and decreasing toughness [45]. Varying Zn/Mg ratios imply in different precipitation behaviors



and mechanical properties, as studied by Zou et al. [46], in which they observed that the ageing process is significantly accelerated by increasing Zn/Mg ratio, and the time to peak ageing decreases by a factor of 6 with increasing the Zn/Mg ratio by approximately the same factor. The same work shows that an alloy composed by Al–8Zn–2.8 Mg–1Cu wt% presents the highest ultimate tensile strength (609 MPa), the worst elongation (6.0%), and higher peak hardness (187.6 HV) among the investigated alloys, presenting brittle intergranular fracture. Also, specimens with smaller amounts of Zn (4.8% wt) exhibit transgranular fracture with good elongation.

Machinability of aluminum alloys is most focused in age-hardening families, especially 2000 and 7000 series, due to their larger consumption by aeronautic industry [47]. The improvement in strength that turned possible aeronautic applications is the formation of second-phase precipitates. With them, aluminum alloys can reach yield stress values up to 100 times that of pure aluminum [48]. Besides, the control of precipitates can be decisive to control the surface integrity [49] and machining aspects [50], including the 6000 series alloys. Milagre et al. [49] verified for Al6061 alloy that different thermomechanical processes used to nuclear fuel plates cause tensile residual stresses, besides a reduction in hardness compared to T6 condition. The reasons for their findings are the dissolution of beta phase, the increase of grain size, and the precipitate coarsening. Froehlich et al. [50] compared using drilling experiments the resulting forces of Al6061 alloys with different levels of Pb and Ti additions, and the alloys Al2117 and Al6351 on the cold-worked condition. Although Al6061 alloys have the highest mechanical strengths (338–343-MPa UTS), the presence of alloy elements is able to reduce significantly the drilling forces. In addition, some precipitates helped the machinability in Al2000 series alloys, especially CuAl<sub>2</sub> precipitates.

## 3 Machining parameters of aluminum alloys

### 3.1 Surface integrity

Since the mechanical strength of aluminum is generally considerably lower than that of most steels and cast irons, tool wear is often not high enough to be considered the primary machinability criterion. That said, due to aluminum alloys' high ductility and low melting point, surface integrity is usually the main machinability criterion. Therefore, the surface integrity will be addressed in relation to the surface topography (generally influenced by cutting parameters, in particular, the feed), microstructural changes (generally caused by the heating of the cutting interface), and the effect of mechanical properties on these two parameters.

#### 3.1.1 Surface topography

As stated before, machining aluminum alloys usually lead to relatively low tool wear rates compared to other metals. Because of that, surface topography is usually the most critical machinability parameter, primarily due to the high ductility of the aluminum alloys that leads to high plastic deformation at the cutting interface, and thus may cause high roughness values. Horváth et al. [51] investigated the finish turning of two aluminum alloys (AS12 and AS17) using three types of diamond tools, namely, polycrystalline (PCD), monocrystalline (MDC), and vapor deposition (CVD) synthetic diamonds. The tests were performed with different levels of cutting speed, feed rate, cutting depth, and tool shapes to estimate the arithmetical mean deviation ( $R_a$ ) and maximum height ( $R_z$ ) of the roughness profiles. The authors reported that the models used  $R^2$  to predict  $R_a$  and  $R_z$  for manufacturing process planning, with the cutting speed being the most influential parameter and the harder alloy leading to a better surface finish. Xu et al. [52] evaluated the use of an electrostatic minimum quantity of lubrication (EMQL) in the high-speed milling of AlSi7Mg alloys (Al6000 series) under cutting speeds ranging from 600 to 2400 m/min, feed rates from 0.08 to 0.2 mm/rev, and cutting depth from 0.4 to 1.3 mm, with the results being compared to dry, flood, and conventional MQL lubrication systems. The authors reported that the EMQL system outperformed the other conditions, followed by flood cooling, MQL, and dry machining. The explanation is that the electrostatic lubrication better cooled the surface, reducing the plastic deformation at the cutting interface. Based on this performance, the authors indicated the EMQL as the most sustainable method for lubrication in the high-speed milling of the investigated aluminum alloys.

Yücel et al. [53] evaluated the use of MoS<sub>2</sub> nano-MQL in the turning process of the Al2024-T3 alloy, using uncoated cemented carbide tools, cutting speeds ranging from 300 to 500 m/min and feed rates from 0.1 to 0.3 mm/rev at a constant depth of cut of 1 mm. Machining results of the nano-MQL were compared to dry and conventional MQL conditions. The authors reported that the nano-MQL outperformed the other conditions regarding the average surface roughness, followed by the conventional MQL and dry conditions. The best results were found at the lower cutting speeds and feed rate, with the feed rate with the biggest influence on the average surface roughness. Zhang et al. [54] evaluated the machinability of the Al7050-T7451 alloy under the ultrasonic elliptical turning process, using as parameters cutting speeds ranging from 600 to 1800 m/min, cutting depths from 1.5 to 3.5 mm, feed rates from 0.025 to 0.125, and vibration frequencies from 0 to 25.000 Hz. The authors reported a lower surface roughness when using the ultrasonic vibration-assisted method, with

the roughness for the conventional cutting (0 Hz) up to 4 times the roughness at the highest vibration frequencies.

It is well known that machining can be employed to control the wettability of surfaces for various industrial applications (coating, lubrication, brazing, etc.) [55]. Surface texturing of aluminum and related alloys via machining has been the focus on many studies in the past literature. The studies in general aimed to understand how surface texturing can affect the wettability and ways to optimize it for certain applications. An example of such machining processes includes ultrasonic-assisted machining and laser ablation. Khanali et al. [56] studied the application of low-frequency vibrations during face turning processes, aiming to adjust the tribological characteristics of surfaces. The authors introduced a novel, cost-efficient approach to generate large-scale textures on surfaces. The influence of cutting parameters on surface profile, wettability, and friction coefficient was evaluated, indicating that the density of peaks and valleys predominantly affects the friction coefficient, whereas texture density influences wettability. An optimal configuration was identified at a rotation speed of 45 rpm, which minimized the friction coefficient. On a similar note, Zhao et al. [57] investigated the effect of machining parameters on the microstructure of surfaces milled by single-excited rotary longitudinal ultrasonic twist milling. Their results showed that surface quality improves when the ultrasonic amplitude is 4  $\mu\text{m}$ , and both cutting speed and feed rate have a positive correlation with surface roughness and water contact angle. Interestingly, surfaces machined under ultrasonic mode had higher water contact angles compared to those under normal mode. The difference in water contact angles between surfaces machined at high and low amplitudes was not significant beyond a certain speed. They concluded that the right machining parameters under longitudinal ultrasonic twist processing can reduce surface roughness and modify wettability. Further extending the application of ultrasonic techniques, ultrasonic-assisted turning (UAT) has been employed to generate unique microtextures on titanium implants to enhance cell adhesion. Zamani et al. [58] employed UAT process to create such microtextures to study the effects of vibrations on the developed interfacial ratio (Sdr) theoretically and numerically. Their results showed that the microdimples were influenced by ultrasonic characteristics, including amplitude and direction, as well as cutting speed as shown in Fig. 3. The application of UAT improved Sdr while barely affecting surface roughness. SEM images further demonstrated UAT's potential in manufacturing titanium implants with enhanced adhesion properties for osteoblastic cells, showing greater integrity and extended fibronectin of adhering osteoblasts on textured surfaces. In addition, they found that increasing the cutting speed resulted in higher Sdr by up to 20%.

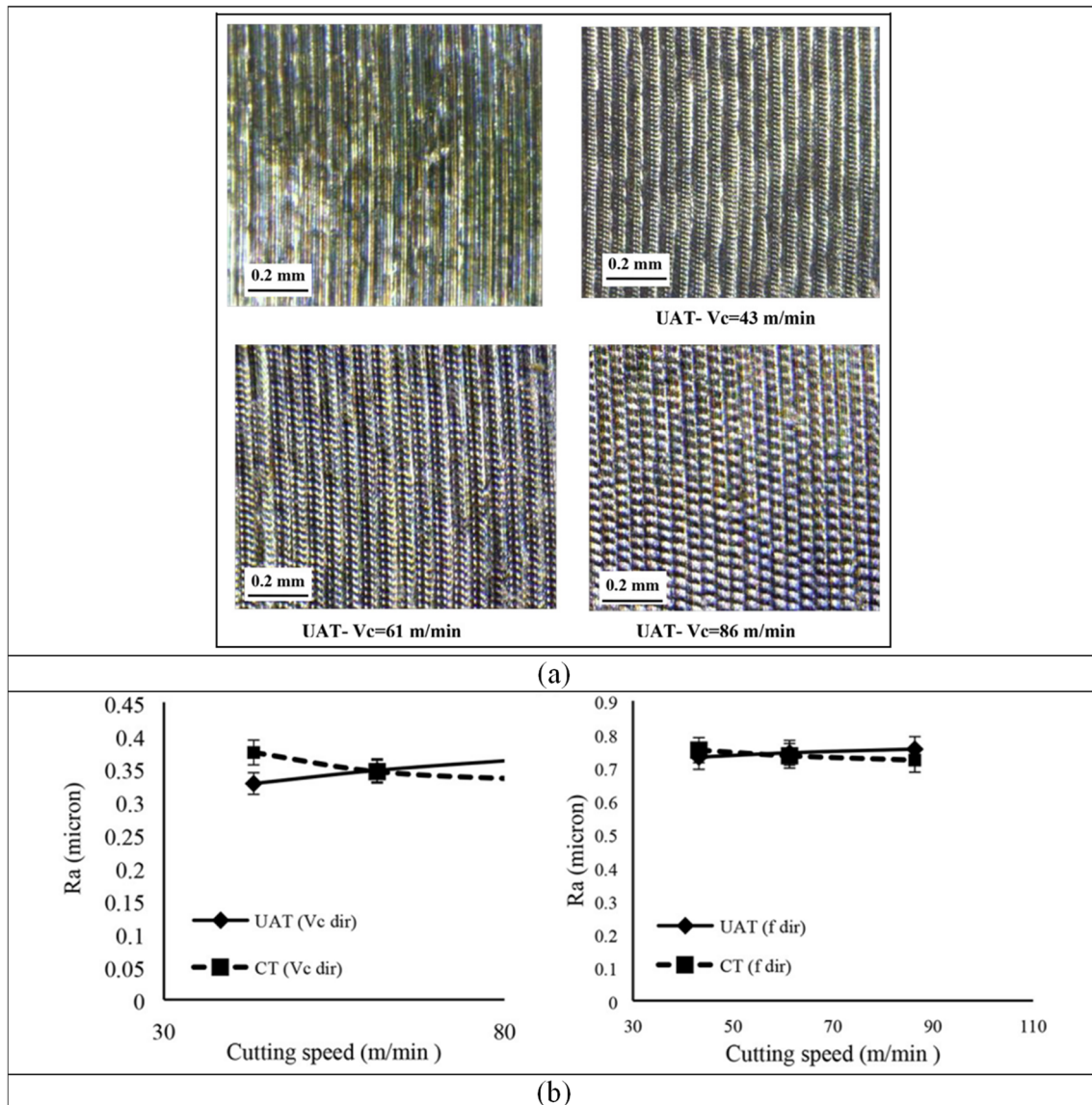
Nouri et al. [55] conducted an experimental study on the wettability of microtextured surfaces created by ultrasonic-assisted face turning. The study examined the effect of process parameters on the wettability of both non-textured and textured patterns. Their results suggest that ultrasonic-assisted face turning (UAT) effectively generates microcavities on flat surfaces. By manipulating process parameters, they could alter the expansion of these microcavities in the cutting direction, thereby increasing the interfacial area between liquid and solid and enhancing adsorption between surface and water as shown in Fig. 4. Consequently, textured surfaces demonstrated superior wettability performance compared to their non-textured counterparts.

### 3.1.2 Microstructural alterations

In general, microstructural alterations are linked to the high plastic deformations present during the chip formation process as shown in Fig. 5. When higher cutting speeds are used (usually to increase productivity, surface integrity, and avoid build-up edge), the cutting temperature also rises, and due to the relatively low melting point of the aluminum alloys, it can also cause microstructural alterations. The microstructural alterations occur due to plastic deformations which cause changes in the shape, length, and thickness of the newly formed micrograins in addition to changes in the machined surface hardness. The effect of machining parameters on the microstructure and hardness of newly machined surfaces varies depending on several factors such as the level of cutting parameters, cutting tool material, coating and its geometry, presence of coolants, type of machining process, and the type of machined alloy, all of which have direct effect on the cutting temperatures and plastic deformations.

Fergani et al. [62] evaluated the effect of the temperature generated during the turning of an Al7075-T6 aluminum alloy regarding hardness and subsurface grain size. The results were modeled using a Hall–Petch-based approach to compute the grain size evolution caused by the rise in cutting temperatures. The machining trials were performed using a PVD-coated cBN insert to avoid the effects of tool wear and the dry condition to simplify the thermal gradient at the cutting zone. The model presented by the authors achieved highly correlated predictions of the grain size and its increase, as well as the hardness in relation to the machining temperatures. Their findings revealed that thermal effects play an important role in inducing grain growth, which softens the material and reduces its hardness as shown in Fig. 6.

Liu et al. [63] studied the nuances of the transformation from crystalline to amorphous caused by the plastic deformation at the nano-machining process of Cu–Al (2000 series) alloys. The phenomenon was evaluated in relation to variables such as material removal rate, plastic deformation, and cutting force. The nano-milling process

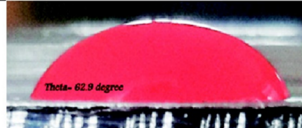
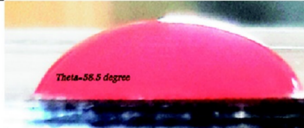
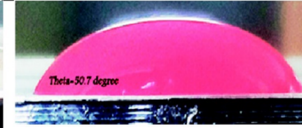
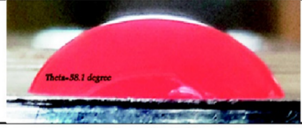



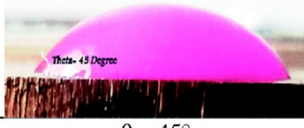



**Fig. 3** Images showing **a** comparison of surface textures according to different cutting speed and **b** results of surface roughness in different directions to cutting speed [58]

was simulated using a diamond tool under cutting speeds of 50 m/s, cutting depth of 3  $\mu\text{m}$ , and initial temperatures ranging from 10 to 600 K. The authors reported that the material mainly deforms as an FCC crystal by the slip of the system [64] (111) when the material is more than 86% crystalline and as an amorphous material when the alloy is less than 86% crystalline. The author further states that dislocation propagation is hindered mainly through the amorphous phase. Imbrogno et al. [65] evaluated the effects of the dry and cryogenic high-speed turning process of the Al7075-T6 alloy on the surface and subsurface integrity. The trials were conducted at different cutting speeds and feed rates using coated cemented carbide tools.

During the trial, the cutting temperature was measured using a thermographic camera. The results showed that increased cutting speed and decreased feed rate lead to lower surface roughness. The temperature increase at higher cutting speeds leads to grain refinement as the material subsurface. Cryogenic cooling lowered the effects of the increased temperature caused by the higher cutting speeds; however, this technique increased the dislocation density at the material subsurface. A summary of some of the previous studies on machining aluminum alloys and notable findings on microstructural alterations and hardness of the machined surface or chips is given below in Table 1.

**Fig. 4** Effect of cutting speed ( $V_c = 56$  m/min and different feed rates on the developed contact angle). CT: conventional turning, UAT: ultrasonic-assisted turning [55]

CT (128 $\mu\text{m}/\text{rev}$ )	CT (205 $\mu\text{m}/\text{rev}$ )	CT (281 $\mu\text{m}/\text{rev}$ )
		
$\theta = 62.9^\circ$	$\theta = 58.5^\circ$	$\theta = 50.7^\circ$
UAT <sub>a1</sub> (128 $\mu\text{m}/\text{rev}$ )	UAT <sub>a1</sub> (205 $\mu\text{m}/\text{rev}$ )	UAT <sub>a1</sub> (281 $\mu\text{m}/\text{rev}$ )
		
$\theta = 58.1^\circ$	$\theta = 46.8^\circ$	$\theta = 42.5^\circ$
UAT <sub>a2</sub> (128 $\mu\text{m}/\text{rev}$ )	UAT <sub>a2</sub> (205 $\mu\text{m}/\text{rev}$ )	UAT <sub>a2</sub> (281 $\mu\text{m}/\text{rev}$ )
		
$\theta = 56.7^\circ$	$\theta = 45^\circ$	$\theta = 44.6^\circ$
(a)	(b)	(c)

### 3.1.3 Mechanical properties

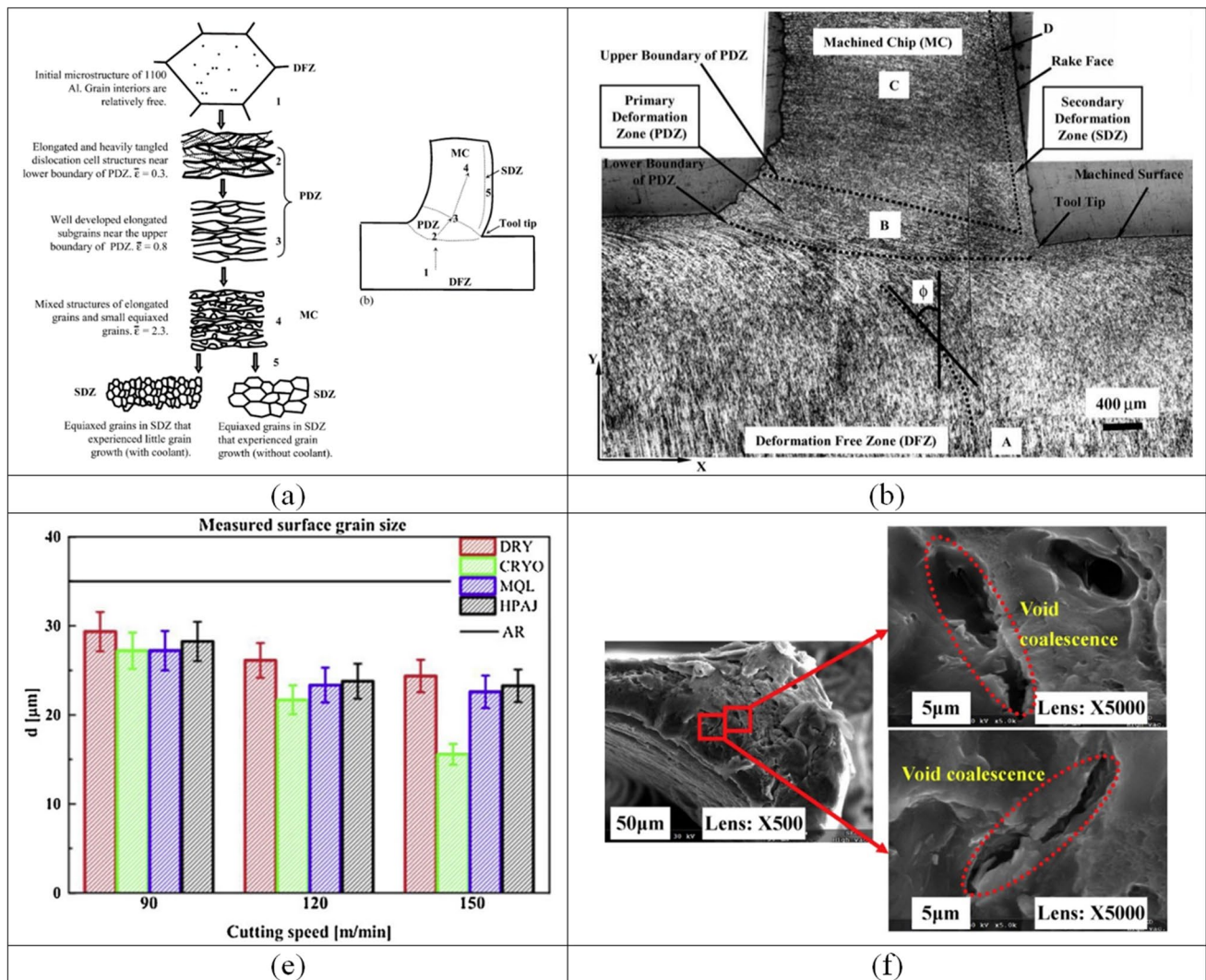
The aluminum alloys can present a wide range of mechanical properties, which can lead to different responses regarding the surface integrity, mainly due to the difference in the plastic deformation at the cutting interface. The manufacturing process can also be a predominant factor regarding the material properties, such as in the study of Guru et al. [69], which evaluated the machinability of an Al–Si alloy (4000 series) manufactured by stir welding. The authors evaluated the machinability of the alloy in the drilling process under cutting speeds ranging from 45 to 75 m/min. The authors reported that the stir-welded alloy led to a higher average roughness than a benchmark Al7075-T6 alloy; however, when the alloy was aged, the  $R_a$  values dropped to less than a half for all evaluated cutting speeds. High plastic deformations are among the most employed methods for achieving nano-grain sizes and are usually obtained using hydrostatic extrusion processes. Skiba et al. [70] evaluated the influence of this technique on the machinability of an Al5083 alloy under cutting speeds ranging from 20 to 250 m/min and feed rates ranging from 0.08 to 0.17 mm/rev. The authors reported that using the hydrostatic extrusion process leads to lower cutting forces and surface roughness, especially at lower cutting speeds. The authors state that the increase in machinability is the result of the alloy's strain hardening, which reduced plastic deformation at the cutting interface. Gonçalves et al. [71] evaluated the influence of copper in the machinability of the Al6351 during the drilling process. The Cu was evaluated at concentrations ranging from 0.07 to 1.93% and was drilled at cutting speeds ranging from 60 to 100 m/min and feed rates ranging from 0.1 to 0.3 mm/

rev. The authors reported that an increase in the Cu content increased the precipitation hardening of the material, increasing the machining forces. However, the authors do not report significant changes in the surface finish of the holes, with a slight tendency to better finish the alloys with higher Cu content.

### 3.1.4 Residual stresses

During any machining process, several factors can play a significant role in the structural integrity of the machined part. Most importantly, thermal and mechanical loadings are induced during the machining process due to different factors as shown in Fig. 7. For example, the contact between the cutting tool and the workpiece generates frictional heat and chip formation which induces thermal loadings in the part [72]. Moreover, the cutting process itself induces mechanical stresses through cutting forces which can also affect the part's integrity. The performance of cutting tools reduces with the increase volume of material removed from the workpiece. As a result, the thermal and mechanical loads would increase, increasing residual stresses and reducing the surface integrity of the machined part [73]. Machining-induced residual stresses can also affect the fatigue life of the machined parts and shorten their service life [72]. It was previously reported that during machining, the increase in compressive stresses on the material's surface improves fatigue life, with varying effects on long-crack and short-crack propagation [74]. In another study, Xue et al. [75] looked into how residual stress influences the machining deformation of thin-walled Al2219 alloy rings used in aerospace products via turning process. The study involved developing





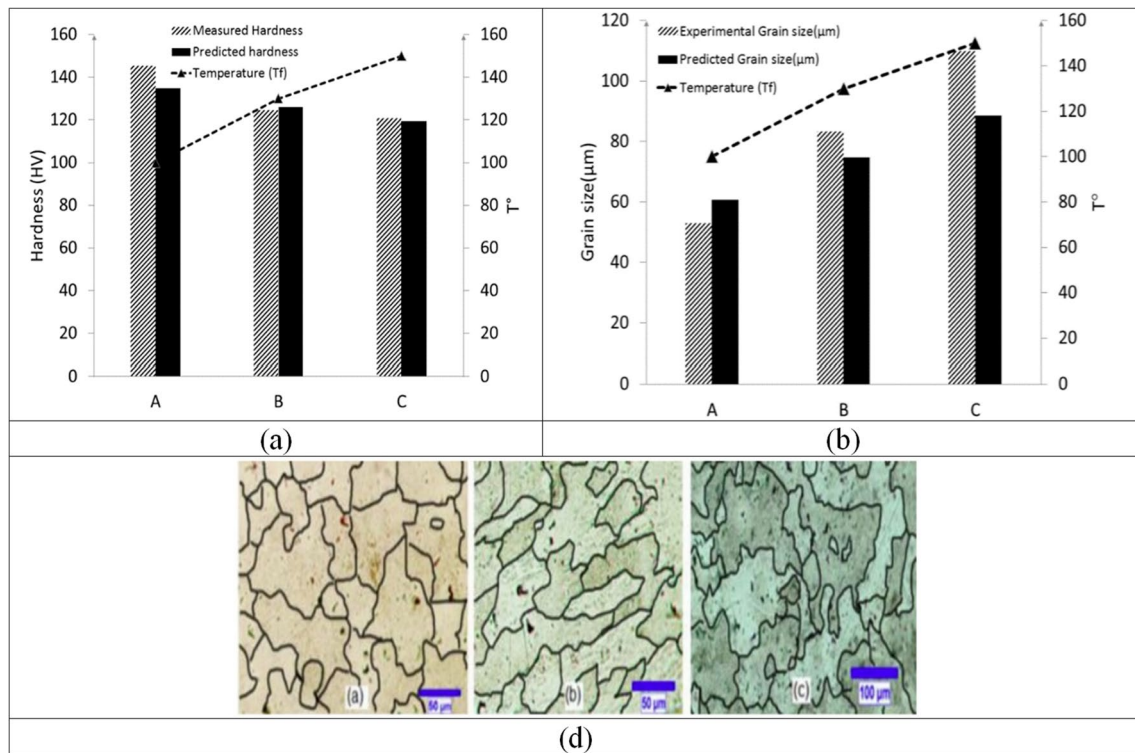
**Fig. 5** Machining of aluminum alloys showing **a** microstructural evolution in aluminum alloys (Al1100) [59], **b** deformation zones during orthogonal cutting [59], **c** effect of coolants on grain size [60], and **d**

fragmented chip obtained under the cutting speed of 7000 m/min for 7050-T7451 aluminum alloy [61]

elasto-plastic numerical and theoretical models to study the distribution of initial residual stress and the law of machining deformation. The authors’ findings highlighted that the residual stress in these rings induces significant machining deformation up to 0.4 mm and induced an elliptical cross section with a maximum ellipticity of 0.52 mm. The workpiece thickness, pre-machining stress levels and their level of asymmetry, clamping setup, type of machining process, and removal strategy can also affect the way residual stress develops during machining and final part distortion [76, 77].

Similar issues exist in non-conventional machining operations that use thermal, electrical, or chemical material removal techniques (i.e., laser machining, wire electrical discharge machining, chemical machining). Li and Wang provided an overview of the current developments in residual stresses and distortion of aeronautical aluminum

alloy, emphasizing the need for controlling these stresses to manage distortion such as in thin-walled parts [8]. However, they pointed out that there are some challenges in measuring residual stresses using non-destructive methods in the industry and highlighted the need for further research in this area. Mathews et al. [79] studied the coupling between inherent and machining-induced residual stress in high aspect-ratio aluminum components during high-speed machining. Their research included experimental and numerical modeling analysis which revealed the existence of a non-linear interaction between these two types of stresses, which depends on the component and stress location. They also found that this non-linear coupling, along with the specific tool path used, greatly influenced the final distortion of the machined part. Machining parameters such as cutting speed and the geometry of the cutting tool significantly affect the formed



**Fig. 6** Effect of temperature on hardness, grain size, and surface microstructure when turning Al7075-T6 alloy [62]

residual stresses in aluminum parts regardless of the machining process [80, 81]. Singh and Agrawal et al. [81] proposed a mathematical model to predict residual stresses in an aluminum alloy. Their model — which considers factors such as cutting conditions and tool geometry — was validated through variance analysis and experimental verification. They conclude that their model is useful for selecting suitable cutting parameters for machining aluminum alloys. The modeling of residual stresses for optimal machining performance is a good practice to improve the structural integrity of the machined parts. However, this practice can be costly in terms of computational power requirements as well as the equipment required to measure residual stresses [82]. In another study, Fuh and Wu [83] proposed a mathematical model to predict residual stresses in Al2014-T6 alloy during milling. Their model, which considered factors such as cutting conditions and tool geometries, was validated through variance analysis and experimental verification. They concluded that their model is useful for selecting suitable cutting parameters for machining the 2014-T6 alloy. They also concluded that the cutting conditions and tool geometry affect the cutting forces, cutting temperatures, and surface microstructure, all of which have a direct impact on the residual stresses. Özbek et al. [84] investigated the effects of an eco-friendly minimum quantity lubrication (MQL) system, based on 100% biodegradable plant material, in the machining of Vanadis 10 steel, commonly used

in the automotive industry. The results demonstrated significant improvements with MQL compared to dry machining in terms of cutting temperature, cutting tool vibration amplitude, tool wear, and average surface roughness. The cutting environment was identified as the most influential parameter on average surface roughness, contributing to 86.31% of its variation. Cutting speed was found to have the most impact on vibration amplitude and tool wear, accounting for 46.22% and 32.41%, respectively. These findings have significant implications for ultraprecision machining of Al components, particularly concerning residual stress and machining performance.

### 3.1.5 Improvement in corrosion resistance

Machining of aluminum alloys promotes the formation of near-surface deformed layers, which causes microstructure modifications that may affect the surface integrity of the part and its corrosion resistance. Machining parameters such as cutting speed and feed rate can promote various forms of localized corrosion, particularly in areas with high residual stresses, refined microstructure, or element segregation and precipitate distribution [85]. There are many types of corrosion which could occur in aluminum alloys and other metals, some of which are summarized in Fig. 8 below:

The effects of corrosion resistance in machined aluminum alloys have been a topic of interest among researchers.

**Table 1** Summary of some studies on machining aluminum alloys and key findings on microstructural alterations and hardness of machined surfaces

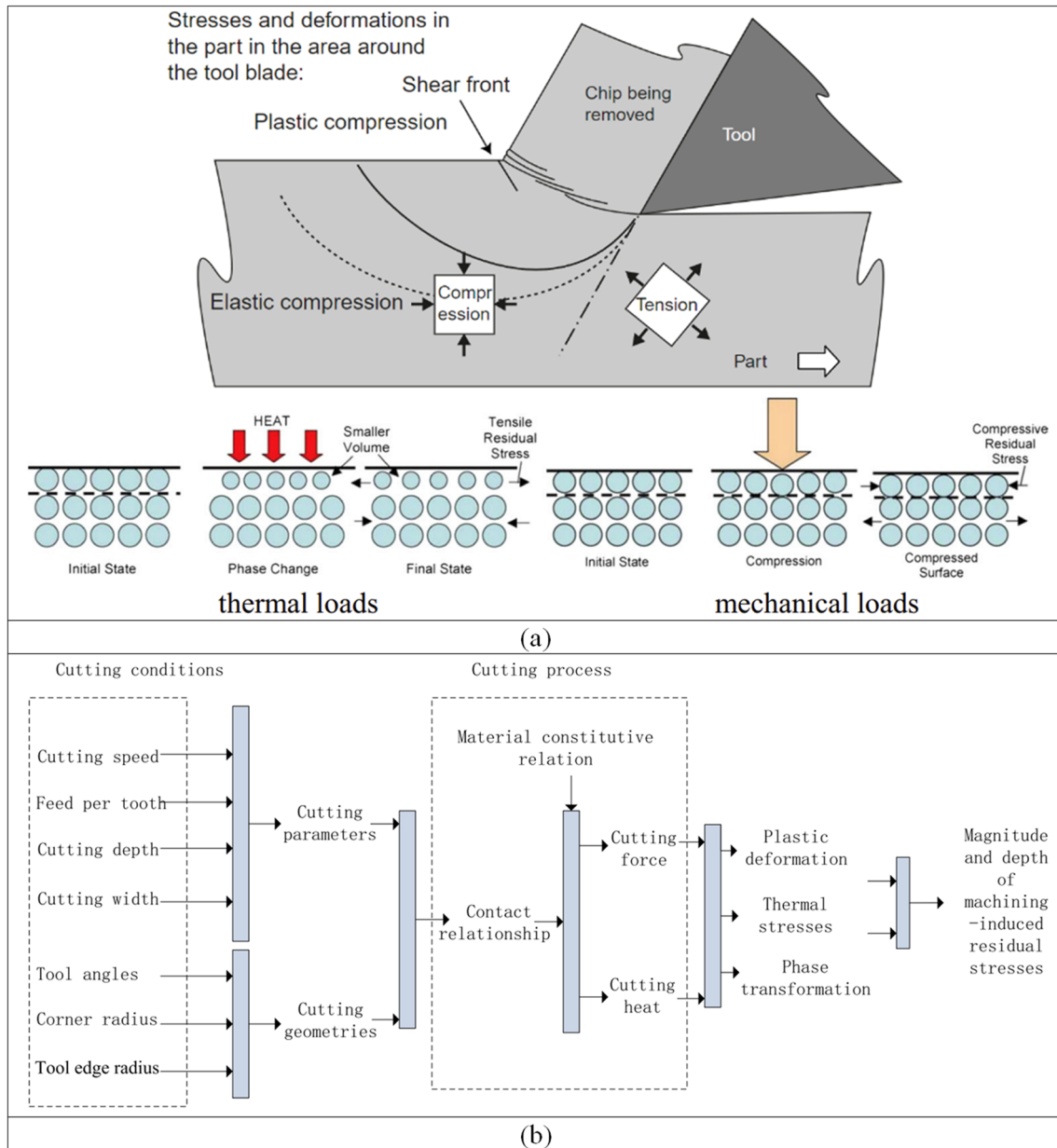
Alloy	Machining process	Effect on hardness	Effect on grain formation	Other	Ref
Al1100	Orthogonal cutting	Up to ↑80%	Elongated subgrains in the PDZ Large equiaxed grains in the SDZ	Chip hardness ↓8% Coolants reduced grain growth in SDZ	[59]
Al7075-T6	Turning	Up to ↓25%	Grain size increased with the increase of depth of cut Grain size increase with cutting temperature	Higher cutting temperatures promoted higher grain growth Increasing depth of cut increased cutting temperature and reduced hardness	[62]
Al7075-T651	High-speed orthogonal machining	Up to ↓5%	Coarsening of precipitates reduces the hardness of machined surfaces	Higher cutting speeds increase the strain gradients at the surface promoting recrystallization Higher cutting speeds caused a decrease in hardness	[66]
Al7075-T6	Turning	-	↓45% in grain size reduction using cryogenic cooling	When higher cutting speeds are used, the cooling/lubrication strategy has an effect on the microstructure	[60]
Al7075-T6	Turning	Up to ↑80%	↓67% in grain size with the increase of cutting speed	Grain size reduced with the increase of cutting speed Variable effect of increasing the cutting speed on the microhardness of the machined surfaces	[67]
Al6061-T6	Orthogonal machining	Up to ↑25% in chip hardness	Strain chip formation is made up primarily of sub-100-nm grains	Flow line chip type was produced Rake angle of the cutting tool affect the chip thickness Chip hardness increased due to effect of deformation temperature	[68]

PDZ: primary deformation zone, SDZ: secondary deformation zone

Liu et al. [87, 88] investigated that the corrosion behavior of machined AA7150-T651 aluminum alloy noticed an increased electrochemical activity — in comparison with the bulk alloy — in the near-surface deformed layer due to the formation of ultrafine grains and the segregation of Mg and Zn alloying elements at the grain boundaries as shown in Fig. 9. Their results also showed that the cutting parameters had a significant impact on the thickness of the near-surface deformed layer ranging anything between 200 and 400 nm [85]. The thickness of the near-surface deformed layer was found to increase with the increase of the feed rate and the cutting speed mainly due to increase in friction force and resulting higher shear stresses. Other studies reported that under the same cutting conditions, the use of coolants during machining such as MQL (minimum quantity lubrication) increases the susceptibility of aluminum alloys to corrosion [89]. In another study, it was found that the machined surfaces become more susceptible to corrosion

when increasing the cutting speed beyond certain limits (i.e., 4000 m/min) during high-speed machining [90]. This was attributed to an increased growth rate of microcracks due to the development of corrosion pits along the direction of the tool marks. Sayadi et al. [91] proposed an innovative method focusing on the Al6061 alloys, utilizing two-dimensional ultrasonic vibrations during the turning process to improve corrosion-related mechanical properties such as roughness, surface defects, microstructure, and corrosion rate. The study concluded that two-dimensional ultrasonic vibrations were more effective than one-dimensional vibrations and conventional turning processes, with the lowest and highest corrosion rates observed in samples machined with these two methods, respectively.

In a more recent study, Sayadi et al. [92] introduced a surface finishing technique called ultrasonic-assisted burnishing (UAB). This technique enhanced the corrosion resistance of AA7075-T6 aluminum alloys without removing any



**Fig. 7** Machining-induced residual stresses showing **a** stresses and deformations formed at the tool-chip interface and **b** cutting conditions that contribute to the formation of residual stresses [8, 78]

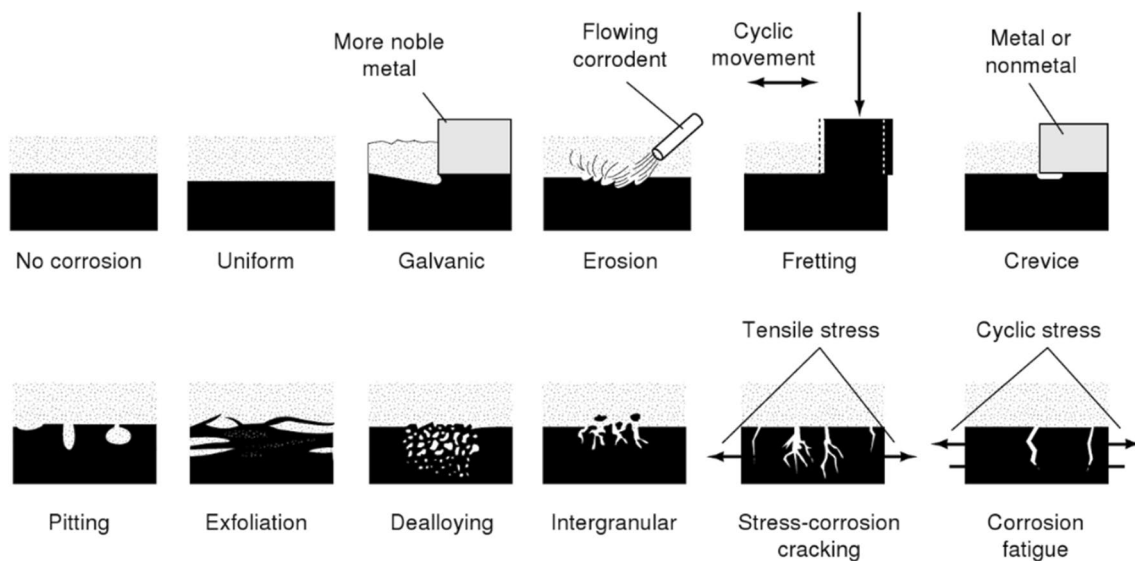
material. The experimental results showed an improvement in surface roughness and corrosion performance after the UAB process, with the best surface achieved at an amplitude of 10  $\mu\text{m}$ . Furthermore, the UAB process led to grain refinement and increased microhardness, both factors contributing to reduced corrosion rate. Liu and Zhou [88] studied the corrosion behavior of AA7150-T651 aluminum alloy post-machining. They observed a near-surface deformed layer with ultrafine grains where  $\text{MgZn}_2$  precipitates were absent but segregation bands rich in magnesium and zinc developed at grain boundaries. These bands promoted localized

corrosion in the deformed layer. Potentiodynamic polarization tests revealed current surges associated with the rapid dissolution of the deformed layer. In immersion testing, it was found that the deformed layer acted as an anode while the bulk alloy served as a cathode during the corrosion process.

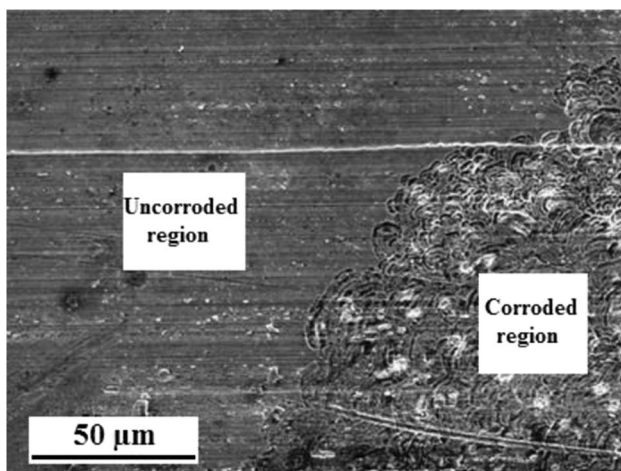
### 3.2 Tool wear and tool life

As previously stated, the relatively low hardness of the Al alloys leads to tool wear not being the main machinability





**Fig. 8** Schematic representations of the typical forms of corrosion [85, 86]



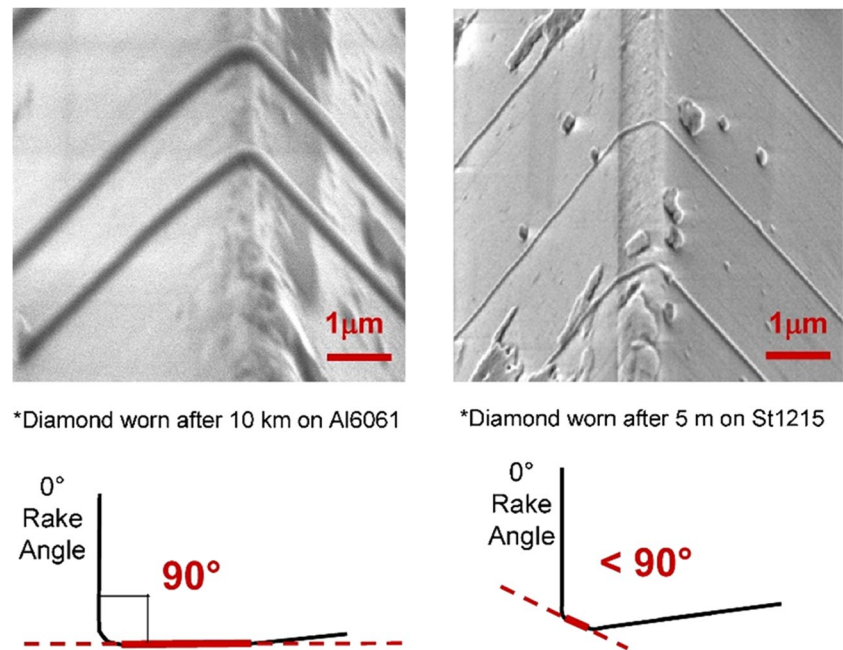
**Fig. 9** SEM image showing regions of corrosion in as-machined AA7150-T651 alloy [85]

problem. Despite that, the optimization of machining parameters remains significant in increasing productivity in the industry, which is the leading research line on this topic. Nouari et al. [93] evaluated the optimization of tool wear in the dry drilling process of the Al2024-T351 alloy. Eight different combinations of tool geometry and coatings were implemented during the tool life trials, for cutting speeds ranging from 15 to 165 m/min and feed rates ranging from 0.04 to 0.4 mm/rev, using uncoated and diamond-coated drills. The authors reported that clearance angles between 6° and 8° lead to better machinability, with the diamond coating significantly increasing tool life. Lane et al. [94] evaluated the tool wear at the orthogonal machining of the Al6061

aluminum alloy compared to the 1215 steel using a diamond turning machine, and the wear was measured using scanning electron microscopy. Using the image and machining force data, the authors determined the Archard wear coefficient. The authors reported that, as expected, the wear rates were higher for steel, with the worn geometry significantly differing for the tools that machined each material, as illustrated in Fig. 10. The difference in the wear was attributed, according to the authors, to the difference in machining forces between the materials and the chemical interaction between the diamond and the steel.

Musavi et al. [95] evaluated the effect of microtextured tools in the machining process of the Al7075-T6 alloy in relation to tool wear and surface roughness. Textures consist of linear grooves perpendicular to the chip flow, under three levels of cutting speeds (100, 125, and 150 m/min), feed rate (0.1, 0.16, and 0.2 mm/rev), and groove distance (100, 200, and 300 μm) under dry and MQL atmospheres. The authors reported that MQL resulted in lower tool wear compared to dry machining, and the use of microtextured tools resulted in a better performance when compared to non-textured ones. The best tool wear and surface roughness results were obtained for the textures with lower groove distance. Liu et al. [96] evaluated vortex-tube cooling in the turning process of A390 aluminum alloys employed in automotive pistons compared to dry machining. Machining trials were conducted under two levels of cutting speed (186 and 300 m/min) and feed rate (0.055 and 0.115 mm/rev) at a constant cutting depth of 2 mm, using cemented carbide inserts. The tool flank wear was measured for all conditions after 400 mm of cutting length. The authors stated that despite the increase in heat-dissipation caused by the vortex tube,

**Fig. 10** Comparison of the tool wear between the Al6061 aluminum alloy and 1215 steel [94]



the overall heat flux did not change significantly. However, using vertex tube cooling reduced tool wear compared to dry machining when combined with the highest cutting speed and lowest feed rate.

### 3.3 Material removal rate

The relatively lower mechanical properties of aluminum alloys lead to higher material removal rates when compared to materials such as steels, titanium, and nickel alloys, which decrease the machining lead time, thus being one of the main advantages. Usually, higher material removal rates are obtained using diamond tools, as it alloys lower/negligible tool wear. However, the higher cutting speeds and feed rates can lead to excessive heating, which may compromise the chip formation as it softens the material; thus, cooling may be required to achieve the desired surface finish without a separate finishing pass. Abas et al. [97] studied optimizing the turning parameters of the Al6026-T9 aluminum alloy under dry and MQL atmospheres. The MQL was delivered at 150 ml/h and 5 bar of pressure at four levels of cutting speed (400, 500, 600, and 700 m/min), feed rate (0.3, 0.4, 0.5, and 0.6 mm/rev), cutting depth (1, 1.5, 2, and 2.5 mm), and positive rake angle of (10°, 15°, 20°, and 25°). The authors reported that the material removal rate influenced tool life and surface roughness for both dry and MQL machining atmospheres, with the main factors being of an insignificant order, the cutting speed, cutting depth, and feed rate. Rathod et al. [98] evaluated the performance of linear (parallel and perpendicular to the chip flow) and square textured uncoated cemented carbide tools in the dry turning process of the Al6063 alloy. The textures have values

of width ranging from 1 to 5 μm, pitch from 5 to 25 μm, and depth from 1 to 5 μm, at a total pater length and width of 700 μm. The authors reported decreased surface roughness and chip thickness as the material removal rate increased. Bansal et al. [99] evaluated the machinability of alumina reinforced (2, 4, and 6%) Al2024 under cutting depths of 1, 1.5, and 2 mm; feed rates of 0.29, 0.32, and 0.35 mm/rev; and cutting speeds of 265, 400, and 535 m/min using both coated and uncoated cemented carbide tools. The authors reported that the material removal rate decreases with the alumina content and increases with the cutting speed and feed rate. Manjunath Patel et al. [100] investigated the influence of material removal rate on the surface quality at the turning process of the Al7075 alloy using CVD-coated cemented carbide tools (TiCN–Al<sub>2</sub>O<sub>3</sub>–TiN). The machining parameters were divided into ten levels combining different values of cutting speed (from 117 to 281 m/min), feed rate (from 0.11 to 0.18 mm/rev), and MRR (9.94 to 30.76 cm<sup>3</sup>/min). Using a surface response method based on a central component statistic design, the authors reported that the lowest surface roughness, circularity, and cylindricity errors were found for an MRR of 28.63 cm<sup>3</sup>/min, with the increase in cutting speed significantly increasing the MRR.

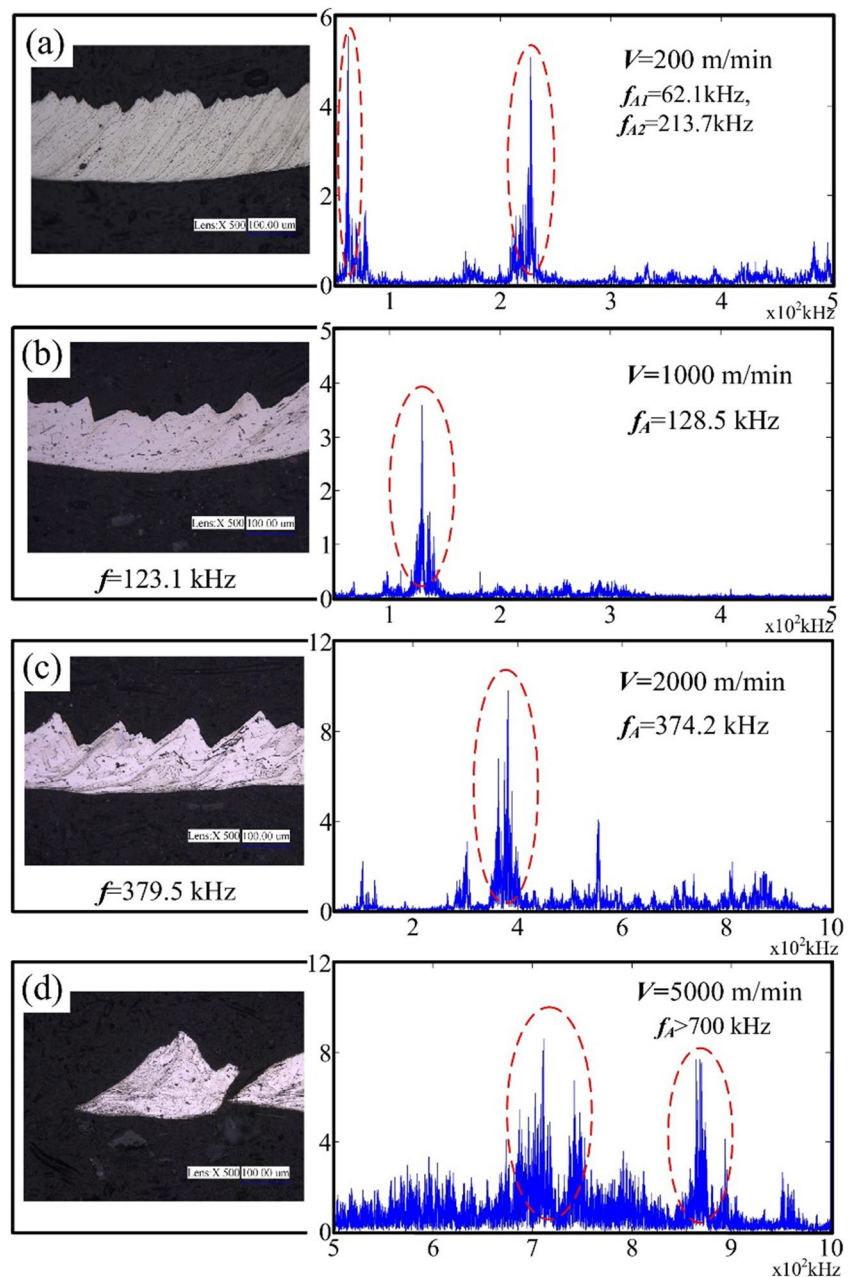
### 3.4 Chip morphology

Due to its inherent ductility, most aluminum alloys tend to present problems regarding chip morphology, usually related to the formation of long chips that can hinder the process due to cutting fluid blockage, chip interference into the cutting interface, and risks related to machine-tool damage and operator safety. Among the techniques

employed to increase the performance in chip morphology are using chip breakers, surface textures, cutting fluids, and optimization of machining parameters. Barzani et al. [101] evaluated the machinability in the dry turning process of Al–Si–Cu aluminum alloys (7000 series) with bismuth (Bi) and antimony (Sb) addition, using PVD-TiN-coated cemented carbide inserts under cutting speeds ranging from 70 to 250 m/min and feed rates ranging from 0.05 to 0.15 mm/rev at a constant cutting depth of 0.5 mm. The addition of Bi and Sb did not significantly influence chip morphology; however, the presence of Bi hindered the BUE formation, and the Sb addition increased the BUE size. Xu et al. [102] evaluated the microend-milling

process of the Al2024 using Ti(C<sub>7</sub>N<sub>3</sub>) cermet and cemented carbide tools under feed rates ranging from 0.5 to 2 μm/z at a spindle speed of 30,000 rev/min and cutting depth of 100 μm. The authors indicate that the chip formation mechanism primarily consists of ploughing at lower feed rates, leading to irregular-shaped chips. As the feed rate increases, the chip formation tends to microcutting, as the shearing process at the cutting interface becomes more stable. Wang et al. [103] studied the chip formation in the high-speed milling process of the Al7050-T7451, employing cutting speeds ranging from 50 to 8000 m/min, at a constant feed rate of 0.1 mm/z, and a cutting depth of 2 mm. As illustrated in Fig. 11, the chip morphology

**Fig. 11** Chip cross sections in the machining process of the Al7050-T7451 and the correspondent acoustic emission signal: **a** 200 m/min, **b** 1000 m/min, **c** 2000 m/min, and **d** 5000 m/min [103]



evolves from continuous to serrated and segmented. This can be explained by the increase in the shear rate caused by the increase in cutting speed, which was also correlated with a specific band of acoustic emission.

Eapen et al. [104] evaluated the differences in chip morphology in the turning process of the Al6063 under pre-cryogenic cooled and dry environments. Machining trials were performed under cutting speeds ranging from 70 to 175 m/min and feed rates ranging from 0.2 to 0.4 mm/rev at a constant depth of cut of 2.5 mm. For the machining, trials were also employed two different inserts, one for general purpose CNMG 120408 MPTT 5100 and one specific for machining aluminum alloys CCGT 120408 FC K10-1. The authors reported that cryogenic cooling improved the performance of the general-purpose tool regarding chip morphology; however, it was ineffective in improving the same aspect for the specific purpose tool.

#### 4 Improvement of machinability on aluminum alloys on different aspects

In the manufacturing field, there is an increase in demand for higher productivity at a lower cost. Recently, application of aluminum alloys in manufacturing industry has increased considerably, due to its excellent exhibition of properties — corrosion resistance, high reflectivity, low emission power, and high thermal and electrical conductivities. The applications of these alloys are mainly in aerospace industries, military equipment, and automobile sectors. The aluminum alloys are manufactured through many different processes like casting, forming, and machining. However, aluminum alloys are one of the difficult to machined materials, because during machining, aluminum alloys generate a lot of heat that reduces the machinability and increases the temperature, which ultimately reduces the tool life with increase of temperature. Aluminum alloys can be broadly classified into two categories: wrought alloys and casting alloys; both these categories are further subdivided into heat-treatable and non-heat-treatable types. Cast alloys are cheaply available due to their low melting point and have lower tensile strengths. Machinability of heat-treatable aluminum alloys can be improved by heat treatments as they increase the hardness of the material which will eventually reduce the built-up edge tendency [105]. However, magnesium in aluminum alloys improves corrosion resistance and machinability. Adding manganese to Al–Fe alloys neutralize the effects of iron, but excess of manganese reduces  $\beta$ -phase and promotes  $\alpha$ -phase formation, which decreases the machinability [106]. Further the primary phase Si grains are much harder than any other phases in the microstructure and exert an abrasive influence on the tool and cause tool wear [107]. The silicon seems to be linked together. Due to the brittle nature

of massive silicon plates, alloys with coarse eutectic display poor mechanical properties, particularly poor ductility. The characteristics are further diminished if the alloy is hypereutectic in nature because the proeutectic silicon is coarse and present as cuboids, plates, and needles. The addition of copper to Al–Si alloys improves the strength and machinability as it helps the alloys to respond to precipitation-hardening, but this reduces its corrosion resistance, castability, and ductility. Tool failure due to blockage of flutes is consistent while machining aluminum alloys [108]. Thus, for machining aluminum alloys, tools should have low affinity to aluminum, low friction coefficient, and high hardness [109]. For distortion-free machinability, the residual stress of the aluminum plate needs to be controlled. While, the fatigue properties usually decrease with increasing thickness due to microporosity close to the surface [43].

The term machinability describes how easily a workpiece material can be machined into desired outcome with respect to the machine tools and machining processes. Machinability on aluminum alloys include varied factors like surface finish of the workpiece, amount of tool wear with time, chip formation, relative ease of material removal, cutting force, and power required [110]. From economic as well as ecological aspects, it is necessary to improve the machinability of aluminum alloys by using the right combination of cutting parameters, cutting environment, tool geometry and texture, tool material, and the assisted machining processes, which we will further review in the subsections.

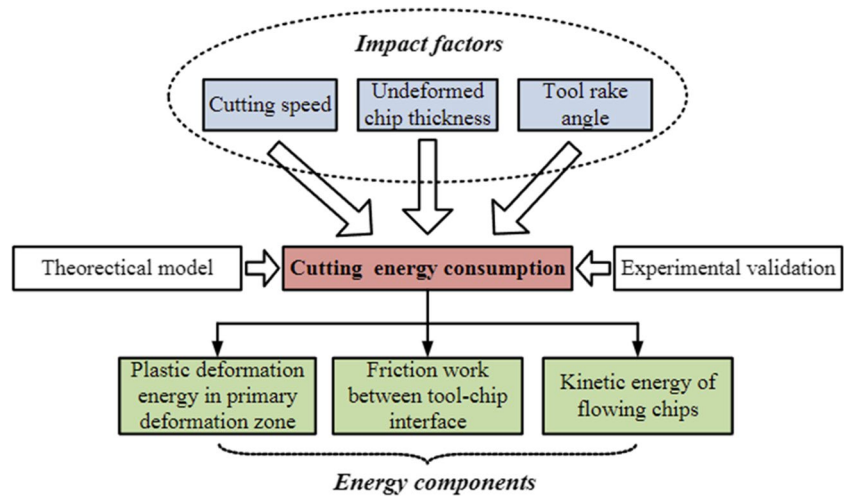
##### 4.1 Improvement of machinability with cutting parameters

Spindle speed, feed rate, and axial depth of cut are a few of the important input parameters on which the quality of the machined workpiece depends. Even machining forces are influenced by many variables like speed, depth of cut, work material, tool material, feed, and a confounded second-order interaction that includes the coolant presence-speed interaction, depth of cut-nose radius interaction, and tool material-feed interaction [64]. Figure 12 shows the standard outline of cutting energy consumption. At low cutting speed (less than 2000 m/min), the energy spent mainly on the plastic deformation for shearing of workpiece. Whereas when cutting speeds are high, the energy is mainly spent on chip flow speed [111].

In machining aluminum alloys, high cutting speeds are preferred as it does not add much in tool wear. High cutting speeds and weak feed rate help the chip breaking and the surface finish [112]. It also avoids built-up edge, which is main factor behind the high cutting force, poor surface finish, and shorter tool life [109]. Due to increased thermal softening, plastic behavior and elimination of build-up reduce the machined surface roughness. In research of

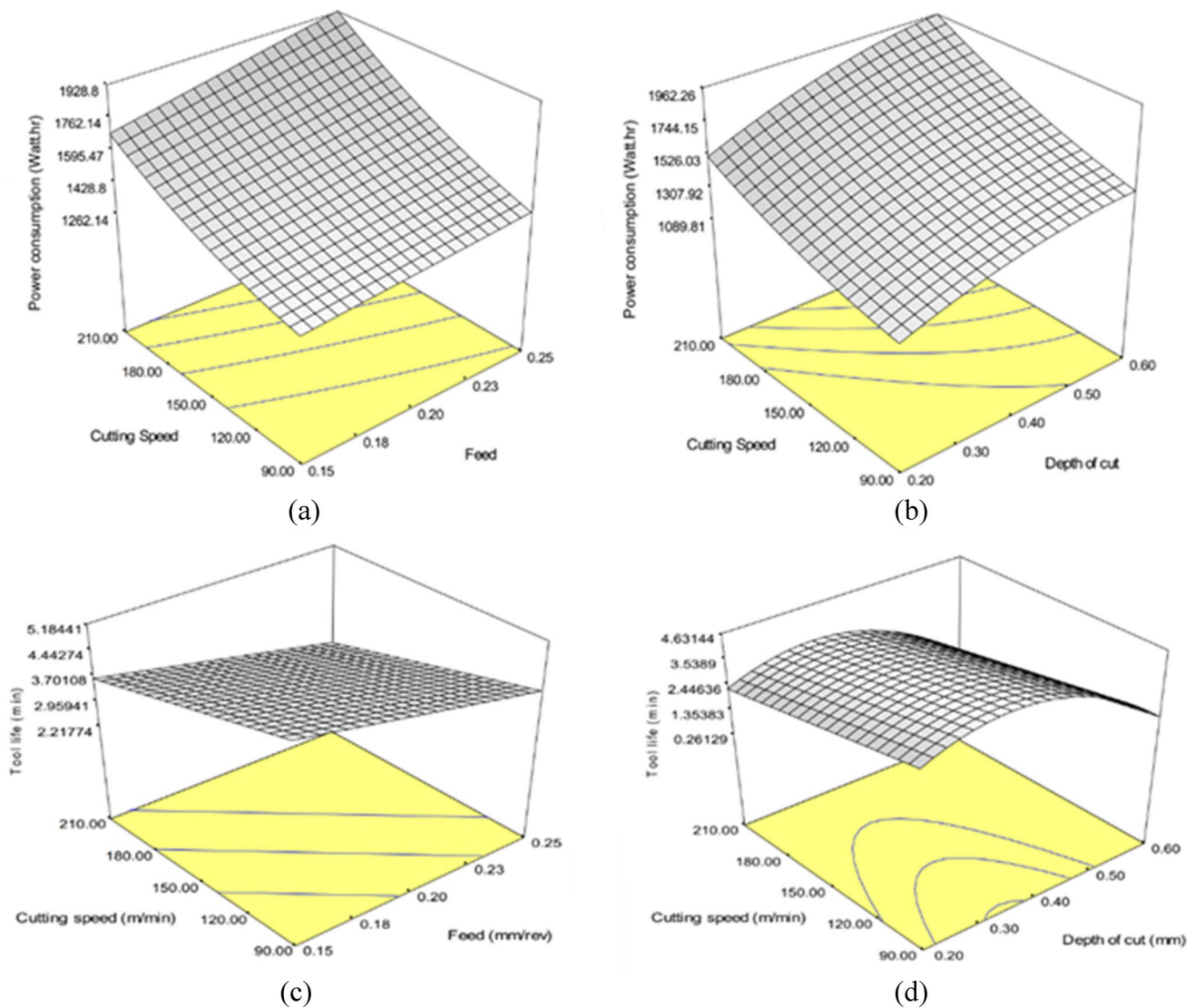


**Fig. 12** Cutting energy consumption outline during high-speed machining [111]



Philippe Revel, the results showed that when the spindle's speed of rotation increases and the feed rate decreases, the average roughness decreases [113]. With decrease in feed rate, surface roughness decreases due to less chatter [114]. In Agustina's research, results also showed the same dependencies of cutting speed, feed rate, and surface roughness; in addition, the parameter of feed rate is the more influential factor for surface roughness. Moreover, the study showed that the shorter and flexible chips were desirable for safety as well as surface roughness [115]. Further material removal rate is better when machining speed is high, and it saves power of machining process. A higher material removal rate is desirable, but it causes the tool to be heated, results in wearing, and degrades the surface quality. Also, the power consumption increases with cutting speed and material removal rate. Bhushan researched on Al7075-15 wt% SiC composite to find the optimal parameter for minimizing power consumption and maximization of material removal rate. Figure 13(a), (c) is a 3D graph whose slope shows the rate of change of power consumption and tool life with varying cutting speed and feed rate, respectively, while Fig. 13(b), (d) slope shows rate of change of power consumption and tool life with varying cutting speed and depth of cut, respectively [116, 117]. Axial depth of cut is directly proportional to machinability. When it increases, the length of flute engagement increases, which results in more cutting force and thus reducing the machinability [118]. The machinability could be improved by decreasing the temperature during machining. Yousefi et al. [119] experimentally demonstrated machining of aluminum alloys using a machine tool with an active magnetic bearing spindle and showed that on increasing the machining speed welded metal from secondary cutting edges disappears, surface finish increases, width of chip thickness decreases, and cutting forces firstly decreases and then increases, resulting in

increase in specific energy consumption. Wang et al. [111] researched the effects of cutting speed, undeformed chip thickness, and tool rake angle on energy consumption and found that the specific energy consumption increases with decrease in tool rake angle; therefore, positive rake angles help to reduce power consumption while considering the surface roughness and tool rigidity. Abbas studied cutting parameters along with the methods of hardening the alloy, using 3-D estimate vectors and artificial intelligence. The workpiece samples were passed through six equal channel angular pressing (ECAP), which is a plastic deformation technique. This resulted in improved properties of the workpiece. As the number of passes through ECAP increases, the grain size reduces, microhardness increases, and ultimate tensile strength increases. On 6th pass, surface roughness decreased (minimum: 76%, maximum: 8%), machining time to remove a unit volume increases for maximum by 6% (minimum: unchanged), and cost price increases (minimum: 2.8-fold, maximum: threefold) [120]. Unnikrishna Pillai et al. [114] used Taguchi method to get an optimized combination of process parameters. Taguchi method helps to study the effects of various parameters at the same time to evaluate the optimal conditions. The results showed that the tool path strategy is the most important factor for machining parameters. Chuchala et al. [121] cold rolled aluminum plates; the experiments showed that the direction of cold rolling as well as the thickness of plates does not have much effect on the roughness of produced surfaces. Syreyschikova et al. [4] designed an analytical model based on index of machinability, which is a ratio of performance of the grinding belt and depth of cut, to choose the grinding belts for the operations. This methodology helped to decrease labor intensity by 4.5 times. Hence, the machining parameters influence the machinability to a very great extent. The various relationships between the different aspects like feed rate, cutting



**Fig. 13** Effect on power consumption due to **a** cutting speed and feed and **b** cutting speed and depth of cut. Effect on tool life due to **c** cutting speed and feed and **d** cutting speed and depth of cut [116]

speeds, and the output parameters like surface roughness, cutting force, and power consumption help to optimize the machinability of aluminum alloy. The different work associated with vibration sensors is shown in Table 2.

#### 4.2 Improvement of machinability with cutting environment

For better machining and quality of produced surface, friction between the rake face of the tool and newly formed chip is an important factor. The chip formed has a smooth metallic surface, which comes in a contact of rake face, thus undergoes a very high normal stress. This condition gives rise to strong adhesion between chip and the tool, governed by the high ductility and low melting point of the material.

Due to this adhesion shear increases in the secondary shear zone, the ideal geometry of the machining tool deforms, and thus the tool cannot perform cutting efficiently and reduces the surface finish [53]. To reduce this adhesion, cutting fluids are used, as it forms a low shear strength boundary film [123]. Liew experimentally showed that low-speed machining of aluminum alloys while using tetrachloromethane and ethanol vapors under regulated pressures using high-speed steel tools reduces cutting forces by increasing vapor pressure till some critical pressure [124]. The cutting fluids are also necessary while machining aluminum alloys because the aluminum alloys have high thermal conductivity, the material heats up during machining and undergoes deformation, coolants help the material to maintain the temperature, but it generates a built-up edge, which is illustrated in

**Table 2** Improvement of machinability of aluminum alloys with cutting parameters

Ref	Process	Workpiece material	Tool material	Different aspects	Results
[115]	Turning	Al7050-T7 and Al2024-T3	TiN-coated tools	<ul style="list-style-type: none"> <li>• Surface roughness and chip morphology</li> </ul>	<ul style="list-style-type: none"> <li>• Surface finish increases with the reduction in feed and descent in machining speed</li> </ul>
[116]	Turning	Al7075-15 wt% SiC composite	6615-grade tungsten carbide	<ul style="list-style-type: none"> <li>• Power consumption and tool life</li> </ul>	<ul style="list-style-type: none"> <li>• Cutting speed: 90 m/min; feed rate: 0.15 mm/rev; depth of cut: 0.2 mm; nose radius: 0.42 mm; power consumption: 1116 Wh; tool life: 6.6 min</li> </ul>
[117]	Turning	Al7075-15 wt% SiC composite	6615-grade tungsten carbide	<ul style="list-style-type: none"> <li>• Tool wear and material removal rate (MRR)</li> </ul>	<ul style="list-style-type: none"> <li>• Cutting speed: 210 m/min; feed rate: 0.16 mm/rev; depth of cut: 0.42 mm; nose radius: 0.4 mm</li> </ul>
[111]	High-speed orthogonal cutting	Al7075-T7451 aluminum alloy	Coated carbide inserts	<ul style="list-style-type: none"> <li>• Specific cutting energy</li> </ul>	<ul style="list-style-type: none"> <li>• Positive rake angle considering surface quality and tool rigidity</li> </ul>
[114]	End milling	Al6005 alloy	Single flute AZSTAR uncoated solid carbide	<ul style="list-style-type: none"> <li>• Optimization of multiple-response characteristics using Taguchi-Grey relational approach</li> </ul>	<ul style="list-style-type: none"> <li>• Spindle speed: 14,000 rpm; feed rate: 600 mm/min; tool path strategy: Raster</li> </ul>
[119]	High-speed cutting	Aluminum magnesium alloy	Tungsten carbide	<ul style="list-style-type: none"> <li>• Surface quality</li> </ul>	<ul style="list-style-type: none"> <li>• Welded metal disappears when cutting speed is more than 200 m/s; minimum surface roughness, i.e., less than 1 μm at cutting speed: 260 m/s</li> </ul>
[122]	Turning	Aluminum alloy Al2011	42 CrMo (Alloy Spring Steel)	<ul style="list-style-type: none"> <li>• Optimization of parameters using Taguchi method</li> </ul>	<ul style="list-style-type: none"> <li>• Shaft speed: 356 rpm; feed rate: 0.418 mm/rev</li> </ul>
[120]	Turning	Al6061 alloy	Carbide-VCGT160404 FN-ALLU	<ul style="list-style-type: none"> <li>• Surface roughness, MRR, and finish turning costs</li> </ul>	<ul style="list-style-type: none"> <li>• For optimum value of 0.800-μm surface finish, 0.341-min/cm<sup>3</sup> time taken to remove a unit volume of material and finishing cost of 6.955\$ at 200 m/min of cutting speed, 0.2 mm of depth of cut, 0.103 mm/rev of feed per revolution</li> </ul>
[121]	Face milling	AW-6082-T6 alloy	Cemented carbide	<ul style="list-style-type: none"> <li>• Surface roughness</li> </ul>	<ul style="list-style-type: none"> <li>• S#3 strategy: (asymmetrical material removal) minimum surface roughness</li> <li>• S#2 strategy: (symmetrical material removal) maximum surface roughness</li> </ul>
[4]	Grinding and polishing	Cast Al alloys	Grinding belt	<ul style="list-style-type: none"> <li>• Performance of tool, depth of cut</li> </ul>	<ul style="list-style-type: none"> <li>• Labor intensity of machined cast Al alloys decreases by 4.5 times</li> </ul>

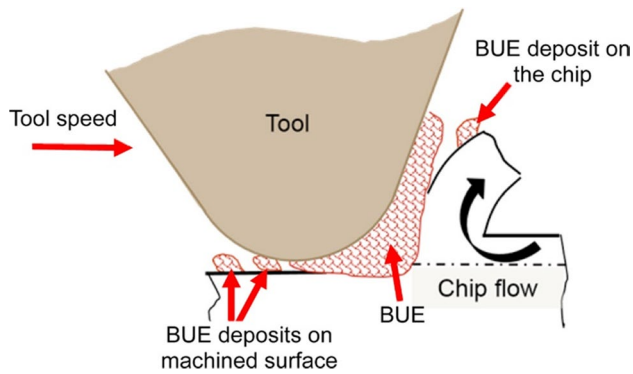


Fig. 14 Built-up edge illustration [125]

Fig. 14. It is economical but hazardous in nature and hard to dispose of.

The consumption of cutting fluids is reduced by using mist lubrication, which gives better machining at high cutting speed and feed rate — but it causes respiratory problems for the workers [126, 127]. Huseyin et al. [128] studied the effects of cutting fluids with nano-silver and borax additives and found that the additive is successful in reducing the surface roughness but not cutting forces. Thus, recently much research has been focused on optimizing dry machining. The main challenges for dry machines are to limit the heat generation during machining, ease of material, or chip removal. Without coolant, the conditions of pressure and temperature produce diffusion in tool-chip contact region of machined aluminum material and cobalt tools [129]. Thus, to enhance dry machining operation different tool coatings under varied cutting conditions must be used, which is further discussed in Sect. 4.4. The specific requirements for dry machining can be eliminated by using semi-dry operations.

Another cutting fluid which is used in small volume, in the form of mist as per requirement, is known as minimum quantity lubrication (MQL), which leads to environmental as well as economic benefits. The MQL covers the interface

of the tool and the workpiece with a very thin layer of lubricant, which reduces friction and the heat which comes from it. N. R. Dhar experiment results showed that MQL reduces the cutting temperature, dimensional inaccuracy, better chip formation, and tool-chip interaction, than that of conventional machining with flood cutting fluid supply. N. R. Dhar et al. [130] compared dry, MQL, and flooded coolant conditions in different cutting speeds for machining using diamond-coated carbide inserts. Figure 15 shows the variation of cutting force with varying cutting speed under the different cutting environments found in the study. MQL was the most economical with less tool wear. However, the material adhesion on the tool-chip interference depends on the amount of coolant used and cutting forces depends on the coolant system. The coolant is required for the quality of surface obtained [131].

Batista evaluated the adhesion wear in dry machining only and found that the material adherence on the cutting edge is mainly due to the cutting speed; when cutting speed and depth of cut is low, thick layer appears on the cutting edge [132]. Seyed A. Niknam [133] assessed the influence of cutting parameters on the machining outputs, which informs that both the surface roughness and chip thickness could be controlled by changing machining parameters. Moreover, the biodegradable cutting fluids with higher viscosity and higher flow rate improved surface finish. Gupta et al. [134] discussed the effect of pure cooling-lubrication strategies like dry machining, nitrogen cooling, and hybrid methods that are nitrogen MQL and Ranque-Hilsch vortex tube (RHVT). The experiments concluded that cooling-lubrication methods improve the surface quality, tool wear, and chip morphology, when compared to dry machining. Moreover, the performance of liquid-based MQL was better than the vapor-based, as the surface finish was better in the former. By using nitrogen-MQL, the tool wear decreases by 101–118%. There were no major changes in chip structures, but the RHVT ensures sustainable machining process, as well as most economical in terms of energy and money.

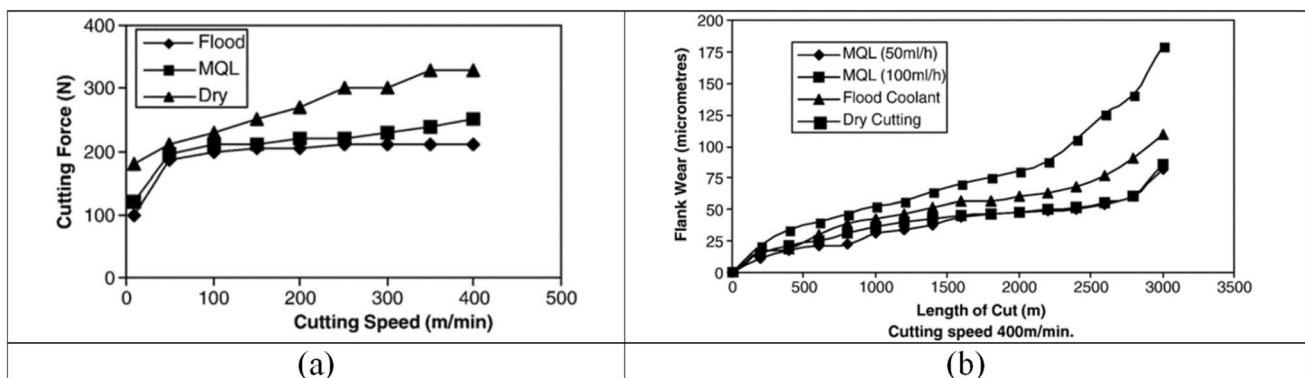


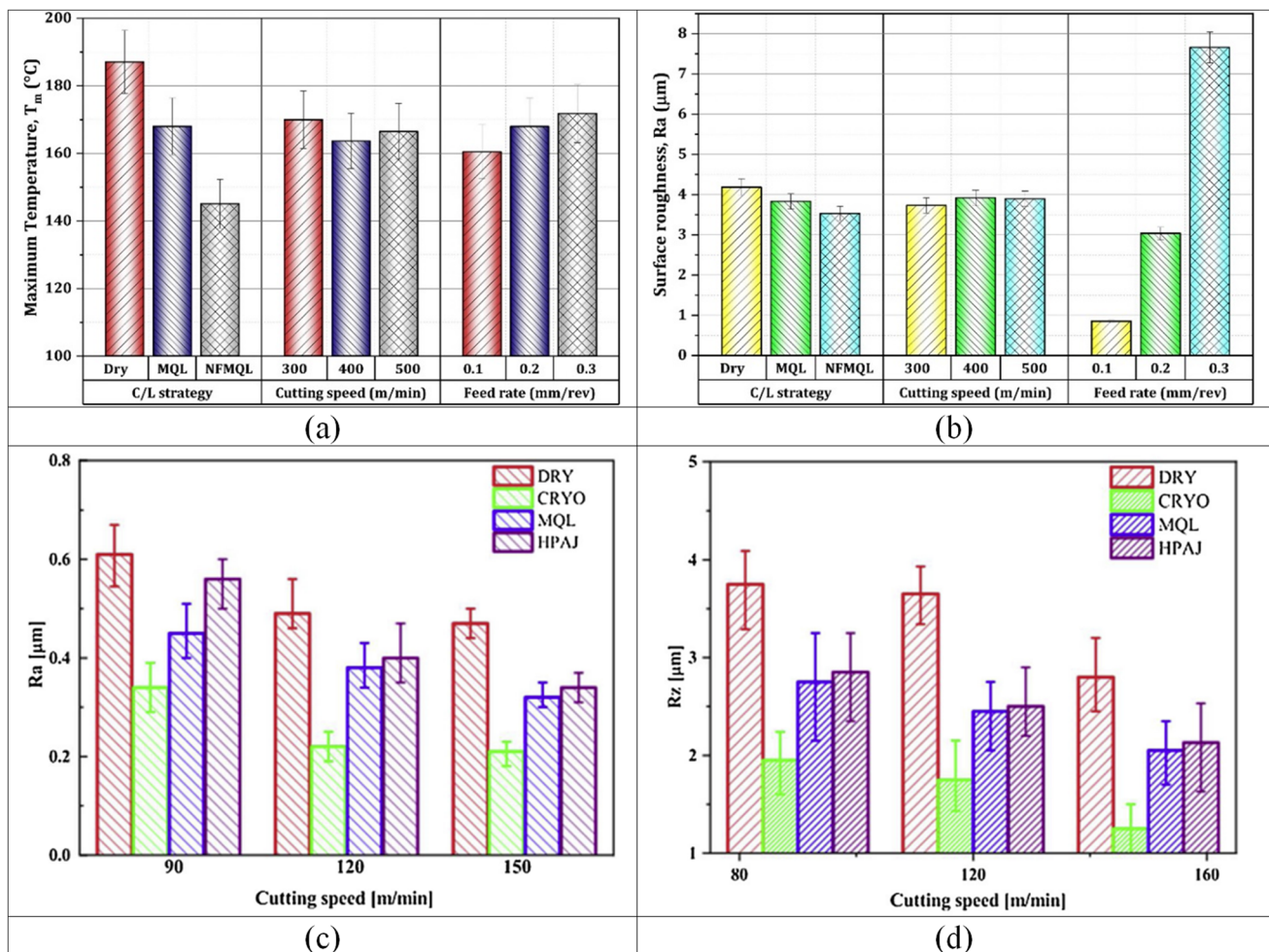
Fig. 15 Variation of **a** cutting force with cutting speed and **b** flank wear with cutting length at 400 m/min [131]



Abas et al. [97] investigated dry and MQL conditions for surface roughness, tool life, and MRR. The results indicated that the feed rate influences the surface roughness the most, tool life by machining speed, while the MRR is affected by cutting speed, depth of cut, and feed rate, former being the most influential. MQL showed minimum surface finish and maximum tool life, when compared to dry machining. However, MRR was slightly higher in dry condition (dry condition: 278 cm<sup>3</sup>/s and MQL: 275 cm<sup>3</sup>/s). Yücel et al. [53] used sustainable cutting environments like dry machining, MQL, and mineral oil-based MoS<sub>2</sub> nano-fluid MQL for machining and investigated different aspects like surface roughness, surface topography, maximum temperature, and tool wear. The results shown in Fig. 16 (a) and (b) conclude that using nano-fluid MQL resulted in the lowest surface roughness, due to the tribo-film layer at the interface, which reduces the built-up edge. Even the temperature and the difference between the peaks and valley on the surface decrease and tool life increases when nano-fluid MQL was used. Similar

results were also reported by Rotella et al. [60] as shown in Fig. 16 (c) and (d) which reported that lower  $R_a$  (<0.4 μm) and  $R_z$  (<2.5 μm) values can be obtained using different cooling technologies, which in return helped retarding the crack initiation.

In cryogenic machining, nitrogen cools the cutting tool and workpiece to reduce the tool wear and increase the tool life. Shane Y. Hong and Zhibo Zhao [135] suggested that lowering the machining process with a cryogenic in cast aluminum, to improve its hardness and resistance to abrasive wear, may reduce build-up edges and improve surface finish of the workpiece. Hence, cryogenic machining and MQL in a mist form is more sustainable, economical, and provides more safety to the operators than the dry machining and flooded lubricant. Even the cooling-lubricant improves the surface roughness and friction between the tool-chip interface. The different work associated with vibration sensors is shown in Table 3.



**Fig. 16** Effect of cooling technology and cutting speed on **a** maximum temperature [53], **b** surface roughness  $R_a$  [53], **c** surface roughness  $R_a$  [60], and **d** surface roughness  $R_z$  [60]

**Table 3** Improvement of machinability of aluminum alloys on with cutting environment

Ref	Process	Workpiece material	Tool material	Different aspects	Results
[123]	Orthogonal cutting	Al 2014	HSS and tungsten carbide	<ul style="list-style-type: none"> <li>• Friction of coefficient, cutting speed, feed, temperature</li> </ul>	<ul style="list-style-type: none"> <li>• The results suggest that there is a synergistic effect between rake face and micro-structural features</li> </ul>
[124]	Orthogonal cutting	Al 2014	HSS	<ul style="list-style-type: none"> <li>• Cutting speed, coefficient of friction</li> </ul>	<ul style="list-style-type: none"> <li>• Tetrachloromethane and ethanol vapor using HSS reduces cutting forces, with increasing vapor pressure until P*(critical pressure)</li> </ul>
[127]	Drilling	Al1050-O	TiAlN-coated carbide drills	<ul style="list-style-type: none"> <li>• Feed forces, torque, power consumption, specific cutting pressure, surface finish, and flow rate of cutting fluid</li> </ul>	<ul style="list-style-type: none"> <li>• For lower feed forces — highest cutting speed: 90 m/min; lowest feed rate: 0.15 mm/rev; cutting fluid flow rate: 100 ml/h</li> </ul>
[131]	Turning	Al6061	Diamond-coated carbide inserts	<ul style="list-style-type: none"> <li>• Cutting forces, surface roughness, and tool wear</li> </ul>	<ul style="list-style-type: none"> <li>• At a higher speed of 400 m/min, surface roughness did not depend on the amount of coolant, but MQL conditions were required</li> </ul>
[132]	Turning	Al2024	Uncoated carbide tungsten inserts	<ul style="list-style-type: none"> <li>• Cutting speed, feed rates, depth of cut, and tool wear</li> </ul>	<ul style="list-style-type: none"> <li>• Cutting speed influences the thickness of adhered chips</li> </ul>
[134]	Turning	Al 7075-T6	Carbide inserts: CNMG120404	<ul style="list-style-type: none"> <li>• Cutting speed, feed rate, tool wear, chip morphology, and cooling condition</li> </ul>	<ul style="list-style-type: none"> <li>• Decrease in surface roughness by 28 to 77% by different methods. RHVT: most sustainable and economical</li> </ul>
[128]	Milling	Al7075-T6	High-speed steel	<ul style="list-style-type: none"> <li>• Feed rate, cutting speed, cutting forces, chip morphology, and surface roughness</li> </ul>	<ul style="list-style-type: none"> <li>• Nano-silver additive effective in lowering surface roughness but not cutting forces; optimum parameters: cutting speed: 75 m/min; feed rate: 0.07 mm/tooth</li> </ul>
[97]	Turning	Al6026-T9	Tungsten carbide insert	<ul style="list-style-type: none"> <li>• Cutting speed, feed rate, depth of cut, surface roughness, surface topography, tool life, and MRR</li> </ul>	<ul style="list-style-type: none"> <li>• For minimum surface roughness: 500-m/min cutting speed, 0.3-mm/rev feed rate, 1.5-mm depth of cut, 25° positive rake angle</li> <li>• For maximum tool life: 400-m/min cutting speed, 0.3-mm/rev feed rate, 2-mm depth of cut, 15° rake angle</li> </ul>
[133]	Turning	Al6061-T6 and Al7076-T6	Carbide inserts: DNGP-432 KC5410 Kenametal	<ul style="list-style-type: none"> <li>• Surface quality, surface roughness, and chip thickness</li> </ul>	<ul style="list-style-type: none"> <li>• Higher viscosity of cutting fluid and flow rate improved surface finish</li> </ul>
[53]	Turning	Al2024-T3	Uncoated cemented carbide inserts: VCGT 160404 FL	<ul style="list-style-type: none"> <li>• Average surface roughness, temperature, and tool wear</li> </ul>	<ul style="list-style-type: none"> <li>• MQL: 10.21% temperature reduced, 8.41% surface roughness</li> <li>• NFMQL: 22.44% temperature reduced, 15.56% surface roughness</li> </ul>

### 4.3 Improvement of machinability with tool geometry and texture

Tool geometry affects the machinability significantly. Figure 17 illustrates the details of tool geometry. With an improper tool geometry, cutting forces varies in machining processes which directly influences the machining output [136]. On machining, aluminum alloys of high toughness generate long chips which wrap around the tool and block the grooves and, thus, result in breakage of the engraving cutter or drill. Hence, large chip flutes should be made in the tool, so that the formed chip can easily flow away. Though the size of chip flutes limits the maximum number of teeth on a cutter, it is necessary to design a tool at an optimum size of flutes. One of another major factors which deteriorate the surface quality is build-up in the cutting edge which makes the cutting edge blunt, resulting in higher load on tool. The build-up can be reduced by increasing the smoothness of the cutting edge by additional polishing or coating. It can also be reduced by designing the tool with specific values of rake and clearance angle. Position angles of rake and cutting edge must be small when machining aluminum alloys. There must be clearance angle to avoid friction between workpiece and tool but small enough to avoid weakness in the cutting edge [112].

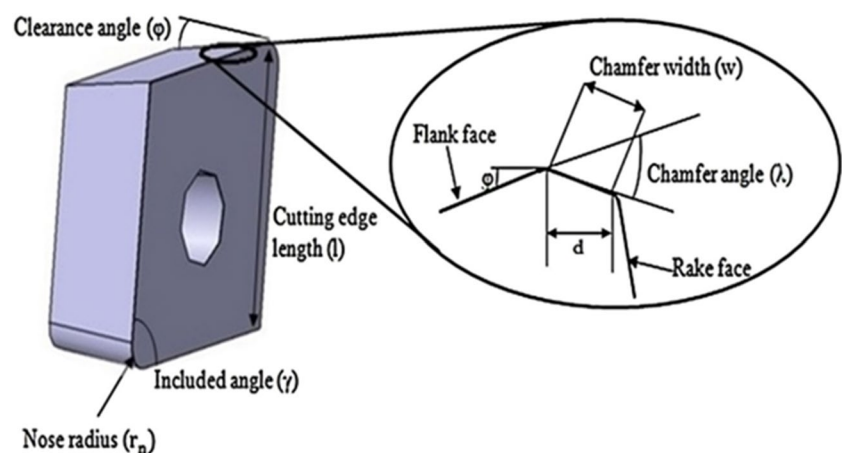
Generally, cast alloys having magnesium, copper, or zinc as the main alloying element are difficult to machine, but it can be improved by using small tool rake angles. Whereas larger tool rake angles, lower feeds, and speeds improve machinability of alloys containing silicon as main alloying element. Non-heat-treatable aluminum alloy strength can be increased by cold work, and then better machining can be done by a sharp tool [138]. Nouari et al. [93] experimented machining aluminum alloys using different tool geometries and concluded that raising helix angle, having large point angle, clearance angle of  $6^{\circ}$ – $8^{\circ}$ , and reducing both the land width and web thickness optimize the machining operation

of drilling. Brinksmeier et al. [139] also tried to investigate the effects of tool geometry and concluded that the use of adapted step drills improves diameter tolerances, surface quality, and tool wear. When designing the tool with large tool nose radii, it will produce better surface finish, but the area of contact of the tool with the workpiece will be also more, resulting in severe wear of tool [116].

Another way to reduce the friction from chip-tool interface is to develop micro/nano-textures on the tool, which reduces the cutting forces and thus heat generation in the cutting zone. Toshiyuki studied the effect of parallel, perpendicular, pit, and dot microtextures at the rake face. The results showed that the parallel and dot type were most effective in reducing the friction force and coefficient of friction. It was concluded that if patten size of microtexture decreases or depth of cut increases, then the tool becomes more effective [140]. Rathod et al. [98] evaluated two types of textures — linear and square, at the rake face which were further coated with  $\text{MoS}_2$  solid lubricant. Figure 18 shows the relationship of cutting forces with cutting speed, friction and normal forces, chip thickness, and surface roughness. The results concluded that in dry machining, textured tools perform better than non-textured tools. In comparison to linear and square, square texture showed better reduction of force; that is, 30% while linear showed 20% with respect to the non-textured tools. Further the chip thickness and surface roughness decrease with the increase in cutting speed, texture depth, and width and decrease in texture pitch.

Further Dheeraj et al. [141] researched and evaluated the performance of solid lubricant-filled textured tools on hole geometry and concluded that the solid lubricant textured tool reduces the built-up formation and eases the flow of chip, thus improving the hole accuracy. The graphite-filled texture gives the maximum hole efficiency of 99%. Graphite has a low volatility, which results in a longer tool life when being machined. Sugihara et al. [142] tried to develop a dimple-textured surface on the rake face of the cutting tool, which effectively suppresses the aluminum adhesion on

**Fig. 17** Tool geometry details [137]



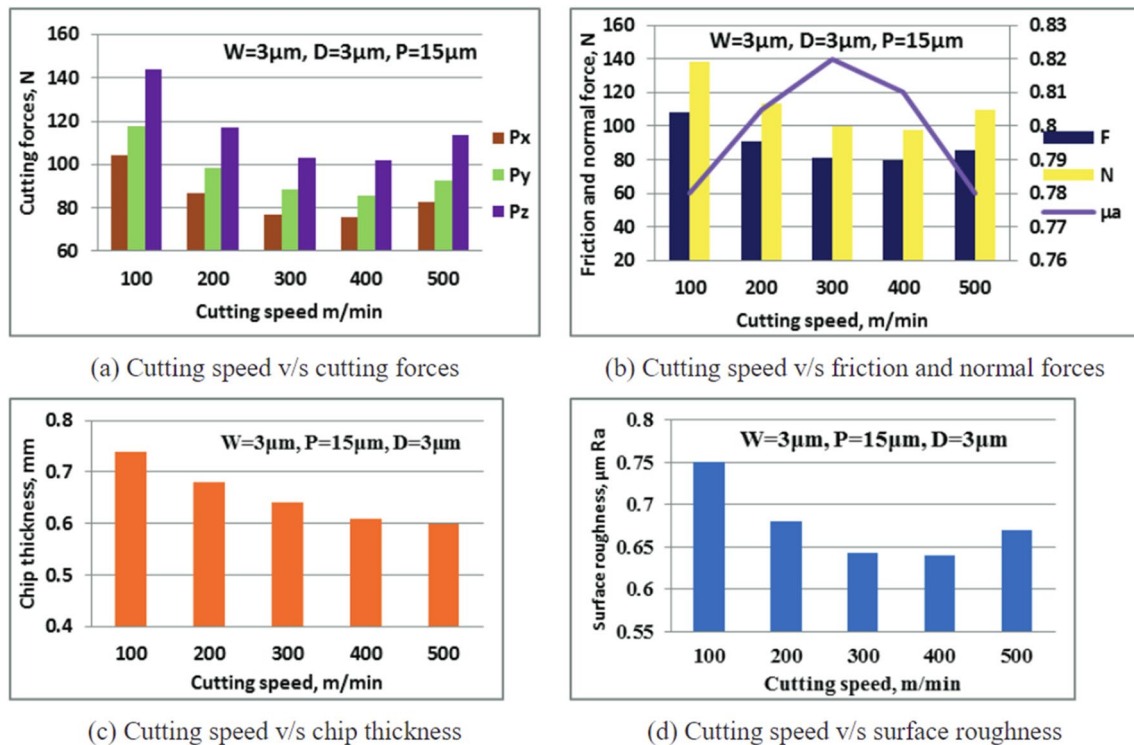


Fig. 18 Influence of cutting speed on different aspects [98]

the tool-workpiece interface. The chip adhesion is reduced to 10% with dimple-textured optimized surface; it facilitates the breaking-off of the adhesion from the tool surface. Al-Tameemi et al. [143] investigated the effect of coating, influence of cutting parameters, hole surface roughness, and dimensional tolerances. The study concluded that surface roughness is maximum when drilling with TiN-coated tool, due to its hardness and high affinity for aluminum. TiN/TiAlN produced the worst hole size, circularity, and cylindricity, especially at low and medium spindle speeds. TiN is most suitable for low machining parameters, while TiN/TiAlN and TiAlN for high machining parameters. Jasinevicius et al. [144] investigated aluminum alloys with different microstructure. The surface roughness was influenced by the material structure like grain boundary, hard inclusions, crystal grain size, and exposed grains. Moreover, the result showed that the reduced thickness of chip causes the increase in friction of coefficient, but the shear angle also decreases with the decreasing chip thickness, which stops the formation of chip, and the machining of surface is by the burnishing effect; this results in more surface roughness. Hence, the review showed that the tool geometry and texture effects the machining of aluminum alloy. The specific optimal geometry improves the machining by reducing friction of coefficient and thus tool wear. Moreover, the textured surface of tool reduces cutting forces and the heat generation in the interface of tool and workpiece. Researchers are trying

to develop intelligent tools for machining aluminum alloys to control vibrations of the tool tip and process a surface with a better surface finish. Dobrota et al. [136] designed and demonstrated the use of intelligent tool, which can be used using cooling-lubrication fluids. The tool damps vibration as well as ensures optimal functional geometry for the machining tool. The results showed a successful reduction of vibration in tool tip and a better surface finish of the machined surface. This was achieved by optimizing the elastic system set under the removable plate. The different work associated with vibration sensors are shown in Table 4.

The threading and grooving processes of Al alloy-machined surfaces have been extensively studied, with a focus on optimization and performance improvement. Khani et al. [145] conducted a study on the threading process of Al7075 alloy using microtextured carbide cutting tools. The objective was to optimize the parameters of these tools using the response surface methodology (RSM), with microtextures fabricated via laser micromachining. The significant factors identified through ANOVA included width, depth, and distance of the microtextures. The optimal levels of these factors were determined, with the microhole-textured tool proving more efficient than microgroove and traditional tools in the threading and grooving process. In a subsequent study by Khani et al. [146], threading in 7075-T6 aluminum alloy was examined using microhole-textured carbide tools and incorporated solid lubricant. The aim was



**Table 4** Improvement of machinability of aluminum alloys with tool geometry and texture

Ref	Process	Workpiece material	Tool material	Different aspects	Results
[93]	Drilling	Al2024-T351	Carbide tool	<ul style="list-style-type: none"> <li>• Tool wear and geometry</li> </ul>	<ul style="list-style-type: none"> <li>• Optimal geometry-raising helix angle, large point angle, reducing land width and web thickness, clearance angle: 6°–8°</li> </ul>
[139]	Drilling	Aluminum, carbon fiber-reinforced plastics and titanium alloys	HSS uncoated, coating of TiB <sub>2</sub> , and diamond	<ul style="list-style-type: none"> <li>• Tool geometry, cutting parameters, and cutting fluids</li> </ul>	<ul style="list-style-type: none"> <li>• Improvements when coatings on the tool is used; for multi-layered materials, MQL should be used</li> </ul>
[140]	Orthogonal cutting	Al6061-T6	Coated ceramic inserts	<ul style="list-style-type: none"> <li>• Friction force, coefficient of friction, cutting forces</li> </ul>	<ul style="list-style-type: none"> <li>• Parallel- and dot-type microtexture decreases the friction force and coefficient of friction</li> </ul>
[98]	Turning	Al6063	Tungsten carbide	<ul style="list-style-type: none"> <li>• Cutting forces, chip thickness, surface roughness, and cutting speed</li> </ul>	<ul style="list-style-type: none"> <li>• Square texture showed better reduction by 30% of cutting forces and linear texture showed 20% in comparison with non-textured</li> </ul>
[141]	Drilling	Al alloy	Tungsten carbide	<ul style="list-style-type: none"> <li>• Built-up edge, hole accuracy, tool wear</li> </ul>	<ul style="list-style-type: none"> <li>• The result showed a decrease in built-up edge formation. The maximum hole accuracy is of 99% while graphite-filled textured tools</li> </ul>
[142]	Face milling	Al5052	Cemented carbide	<ul style="list-style-type: none"> <li>• Chip adhesion</li> </ul>	<ul style="list-style-type: none"> <li>• Microdimples on the rake face reduce the chip adhesion in dry machining</li> </ul>
[143]	Drilling	Al6061-T651	TiN/TiAlN, TiAlN, TiN coating on solid carbide	<ul style="list-style-type: none"> <li>• Spindle speed, feed rate, surface roughness</li> </ul>	<ul style="list-style-type: none"> <li>• Spindle speed influences hole perpendicularity more</li> </ul>
[144]	Turning	Al6061-T6 and RSA Al6061-T6	Diamond tool	<ul style="list-style-type: none"> <li>• Chip thickness, cutting force, thrust force, specific energy, friction coefficient, flow shear stress</li> </ul>	<ul style="list-style-type: none"> <li>• With reduced chip thickness, the friction of coefficient increases and shear angle decreases</li> </ul>
[136]	Turning	Al2024-T351	Low-carbon steel	<ul style="list-style-type: none"> <li>• Optimal functional geometry</li> </ul>	<ul style="list-style-type: none"> <li>• Reduction of vibration in tool tip and a better surface finish</li> </ul>

to improve machining performance for high-quality threaded part production. The results showed improved cutting performance in threading and grooving when compared to conventional tools, with reduced cutting force, radial force, surface roughness, workpiece-tool contact, and operational cost. Incorporating MoS<sub>2</sub> and CNT solid lubricants into the microholes led to further improvements in machining performance. Hoghouhi et al. [147] presented a comprehensive sustainability evaluation in external machining using two new techniques: solid lubricant and tool texturization. The results indicated that these techniques affected the friction force on the raking and clearance faces, resulting in smaller force components. The most efficient machining condition in terms of energy consumption and force reduction was found to be linear texture with solid lubricant, which also improved operator safety. Haddadzade et al. [148] proposed a methodology integrating process planning and scheduling of prismatic components to improve overall system performance. This model considered technological constraints and available machining time on the shop floor, utilizing a multiple process plan (MPP) and overtime to meet delivery deadlines. The study demonstrated improvements in the system's performance in terms of cost and delivery times.

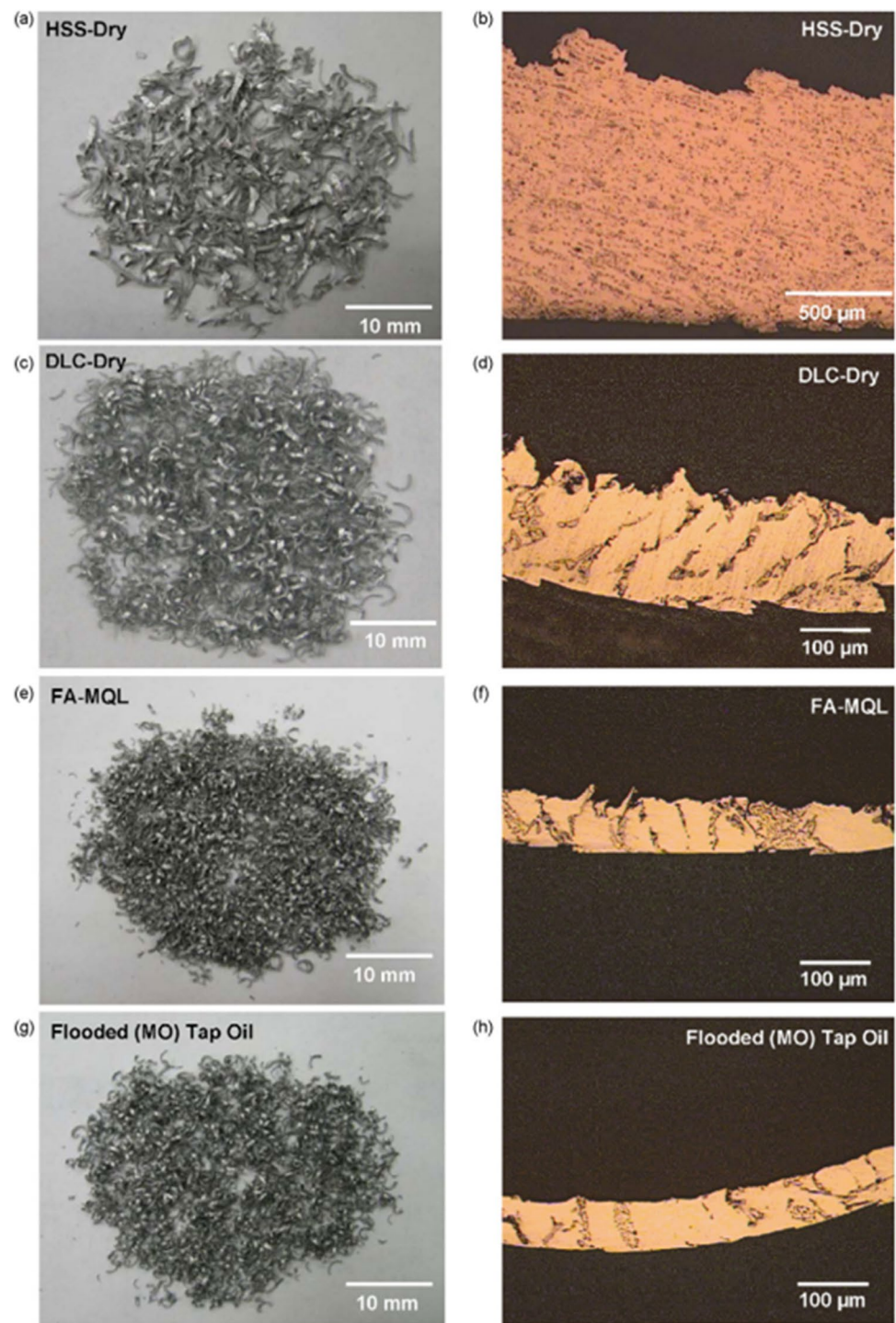
#### 4.4 Improvement of machinability with tool material including coating

Aluminum alloys have good machinability, when lower percentage of silicon is present which is widely dispersed in the structure but when high percentage of silicon is present in aluminum alloys, diamond tools or coating of diamond on carbide tools must be used [112]. As diamond tools have high thermal coefficient, no affinity for aluminum, and fast heat diffusion ability. Diamond coating on rake surface of the tool generates smaller chips, whereas on the flank surface, it produces a rough surface finish of the workpiece. Oles et al. [149] observed that uncoated carbide tools while machining hypereutectic aluminum alloys reach the failure in few seconds whereas the diamond-coated carbide tool in around 10 s and for hypoeutectic aluminum alloys, tool life of uncoated carbide tool is half in comparison to the coated carbide tool. He also suggested that for aluminum metal matrix composites, polycrystalline diamond tools should be used. Due to economic and ecological factors, industries are transitioning to dry machining, which may require the use of higher quality machining tool materials. Thus, diamond is still preferred because of its high wear resistance; it withholds the wear caused by the machining of aluminum matrix alloys in the absence of cutting fluid [93]. For dry machining, some particular diamond-like carbon (DLC) coatings on the tool can also be used as it improve the machining process. DLC has low friction coefficients, high hardness, high chemical stability, and high

wear resistance. Haruyo Fukui et al. [150] prepared DLC film on a cemented carbide substrate by using a vacuum arc discharge with a graphite cathode and compared the machining of aluminum alloys using DLC-coated tool and uncoated tool. The results showed that the uncoated cemented carbide tool had the adhesion of the aluminum material and high friction coefficient whereas coated tool reflected low friction coefficient without any adhesion, and hence reducing machining resistance, and improving machinability of aluminum alloys. Wain et al. [108] showed that graphite-based coating is also effective for improving the machinability of aluminum alloys. In the research blockage of flute is delayed by TiB<sub>2</sub>, Dymon-iC™, and Graphit-iC™ coatings, while the latter coating is most effective for longer tool life. Coldwell observed build-up of workpiece materials on all the tools, though least on Graphit-iC-coated tools, which shows its high anti-adhesive ability and the use of an appropriate hard underlayer showed the improvement in the ability to withstand wear [151]. Though, when there is thin diamond layer on a coated tool, then the tool life is very short, as it easily peels away. When a thick layer is coated, then the wear starts by chipping of diamond grains due to collisions with silicon grains, resulting in diamond grains to fall from the flank face and then deep cracks are propagated. Thus, flank wear in tool is the main factor which influences life of the tool which machining. Hence, improvement in coating causing high resistance to chipping and cracking is necessary for longer tool life [152]. Bhowmick et al. [153] studied tapping of aluminum alloy using dry and MQL machining environment. Figure 19 shows the chip formation in different tools and cutting environment. The results showed that dry tapping with HSS tap caused immediate failure of tool due to severe adhesion and sudden increase of torque. Whereas the DLC-coated taps produced small and stable torque, thus increasing the tool life and quality of thread. Even the friction of coefficient between the DLC-coated tap and the workpiece was less in comparison to uncoated HSS tap, which helped coated tap to generate less heat, preventing built-up edge.

The use of MQL added the benefits of low torques and minimal adhesion [153]. Kalyan et al. [137] investigated the influence of cutting-edge geometry on the machining process at low feed rate and high-speed machining. The results showed that the tangential cutting forces decrease when machining speed increases, due to the thermal softening of the material. While force increases with cutting edge chamfer. Though ploughing force increases more than the tangential when ratio of feed rate to edge chamfer decreases, due to the ploughing effects over the shearing which leads to rubbing. Whereas the surface roughness decreases with increase in nose radius, only when feed rate lies in shearing dominated region. This work will help the industries to choose the feed rate as per the requirement of surface finish [153]. Hence, it is concluded that diamond tools or

**Fig. 19** Chip formation: **a** and **b** HSS dry tapping, **c** and **d** DLC dry tapping, **e** and **f** MQL tapping with HSS, and **g** and **h** flooded tapping with HSS [153]



diamond-coated tools are much more reliable and reduce the cutting resistance. Least built-up edge formation takes place, due to its anti-adhesive effect and thus prolonged the tool life. The different work associated with vibration sensors are shown in Table 5.

#### 4.5 Improvement of machinability with vibration, thermally, and hybrid assisted machining

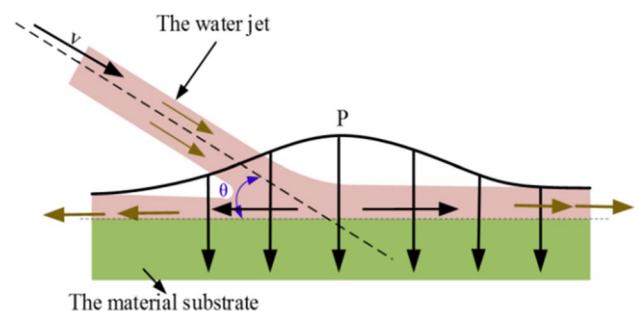
Traditional machining processes have many drawbacks, like deformation and internal stresses, which can be improved by

**Table 5** Improvement of machinability of aluminum alloys with tool material

Ref	Process	Workpiece material	Tool material	Different aspects	Results
[149]	Milling	Al alloys	PCD, diamond-coated carbide tools	<ul style="list-style-type: none"> <li>• Chip geometries, depth of cut, tool wear</li> </ul>	<ul style="list-style-type: none"> <li>• For multiple cutting edges, chip breaker geometries, elimination of depth of cut, and improved performance, then diamond-coated carbide tool is more reliable</li> </ul>
[150]	Milling	Al alloys	DLC-coated tools	<ul style="list-style-type: none"> <li>• Chip flow rate, cutting resistance</li> </ul>	<ul style="list-style-type: none"> <li>• DLC-coated tools reduce approximately 50% cutting resistance; chip flow speed increases while using DLC-coated tool</li> </ul>
[151]	Drilling	BS L168	PVD-coated tungsten carbide tools	<ul style="list-style-type: none"> <li>• Built-up edge and tool wear</li> </ul>	<ul style="list-style-type: none"> <li>• Least built-up was shown on Graphit-iC-coated drills, highlighted its better anti-adhesive effect</li> </ul>
[152]	Cutting	AHS-T6, A390-T6	CVD diamond-coated insert	<ul style="list-style-type: none"> <li>• Wear mechanism</li> </ul>	<ul style="list-style-type: none"> <li>• The CVD diamond film showed excellent abrasion characteristics</li> </ul>
[108]	Drilling	A319	HSS	<ul style="list-style-type: none"> <li>• Friction of coefficient and tool life</li> </ul>	<ul style="list-style-type: none"> <li>• The Graphit-iC coating delay the tool breakage most effectively and have longer tool life</li> </ul>
[153]	Tapping	319 Al	DLC-coated tool	<ul style="list-style-type: none"> <li>• Torque, tool life, heat generation, coefficient of friction, and thread quality</li> </ul>	<ul style="list-style-type: none"> <li>• For performance: 80-ml/h fatty acid-based MQL showed high-quality thread formation</li> </ul>
[137]	Turning	AlMgSi alloy	PCD tool	<ul style="list-style-type: none"> <li>• Feed rate, cutting edge geometry, surface quality, chip morphology</li> </ul>	<ul style="list-style-type: none"> <li>• For best surface finish of 50 nm: lowest feed rate of 0.007 mm/rev at cutting speed between 300 and 600 m/min</li> </ul>

using numerous assisted machining processes. In ultrasonic-assisted milling, after amplification of amplitude is done by ultrasonic horn, the high-frequency ultrasonic vibrations are directed towards the machining tools and components, and the remaining materials are easily removed by the ultrasonic waves owing to its high and focused energy and high impacts. This process can change the surface microstructure, due to the residual compressive stress on the surface imparted by the vibration-assisted machining. It has several benefits over conventional machining like decrease in thrust force and torque, improved tool life, smaller size of chips, and high penetration rate [154]. Lu et al. [155] found that the machining temperature increases with the increase in amplitude and decreases with the increase in frequency. Zhao et al. [156] proposed a longitudinal-torsional coupled ultrasonic vibration machining system. The results concluded that the surface roughness increased with the increase in ultrasonic cutting speed and feed rate, although ultrasonic amplitude is primarily responsible for the roughness. The experiments showed that using a frequency amplitude of 4  $\mu\text{m}$  produced an optimized surface quality and least friction coefficient of the surface. The friction coefficients of surfaces produced by the ultrasonic machining were less than the older processes, resulting in less surface wear. Guo et al. [157] studied the influence of both vibration and amplitude on milling force

and temperature. The study showed that the average machining force and temperature decreases with the vibration at ultrasonic frequency but increases the degree of fluctuations. In the case of amplitude, it depends on the direction vibration applied to the feed. When vibration is applied vertically to the feed direction, the increase in amplitude increases the average milling force, temperature, and the degree of fluctuations, whereas in case of vibrations applied along the feed direction, the increase in amplitude decreases the average milling force and temperature but increases the degree of fluctuations. Moghaddas et al. [154] found through experiments that thrust force and torque increases with the feed

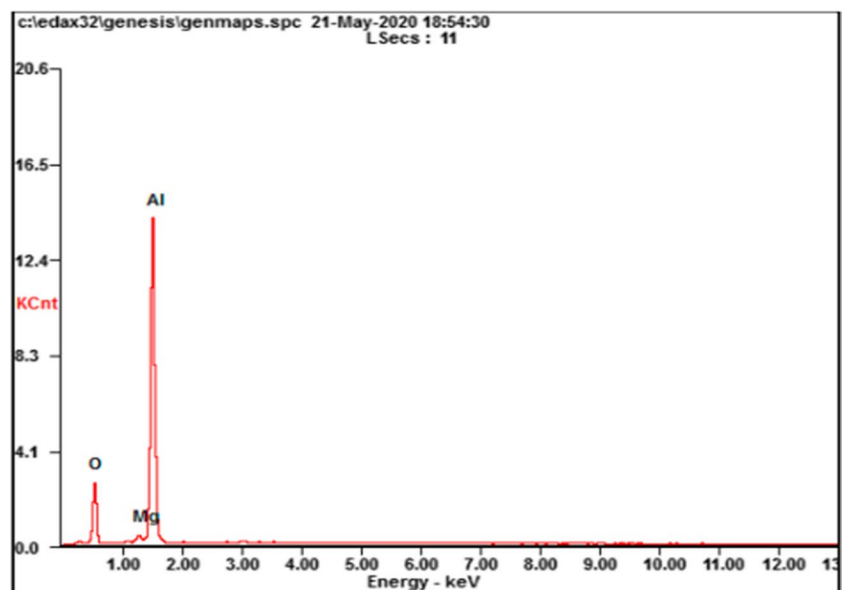
**Fig. 20** Schematic diagram demonstrating impact of water jet [158]



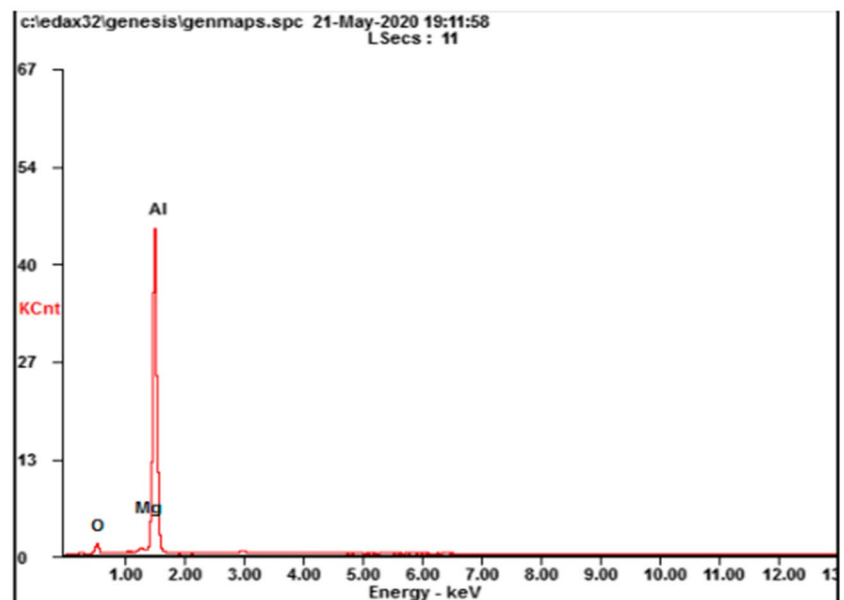
rate and decreases with the increase in amplitude. The latter effect was greater at low spindle speeds. Whereas surface roughness increases with feed rate and decreases with spindle speed. Thus, to improve the surface quality, high spindle speed has a greater influence. Figure 20 illustrates the water jet-assisted laser processing. In this processing there is an addition of a water jet to the conventional laser processing, which gives the benefits of laser processing, as well as remove the slag and debris produced during the process by utilizing the effect of water jet's impact, thereby improving the quality of processed material to some extent.

However, the impact of water jet, while hitting the solid surface, results in water hammer pressure. Chen et al. [158] studied the water-jet-assisted laser machining and found that the processed groove is better, crack free, and less accumulation of slag, when incident angle of water jet is set at  $45^\circ$  and its speed at 14 m/s, laser power at 100 W, and 1.2-mm/s scanning speed as shown in Fig. 21. Hence, assisted machining provides additional characteristics over conventional machining. The relation between the frequency, amplitude, and machining parameters helps to optimize the machining as per requirement. If the right

**Fig. 21** Energy dispersive X-ray analysis of slag at the bottom, processed by laser processing **a** without water and **b** with water jet [158]



(a)



(b)

**Table 6** Improvement of machinability of aluminum alloys with vibration, thermally, and hybrid assisted machining

Ref	Process	Workpiece,material	Different aspects	Results
[156]	Ultrasonic-assisted milling	Al7075	<ul style="list-style-type: none"> <li>• Surface quality and friction coefficient</li> </ul>	<ul style="list-style-type: none"> <li>• 4 <math>\mu\text{m}</math> of amplitude produces optimized surface quality and least friction coefficient</li> </ul>
[157]	Ultrasonic-assisted milling	Al7075-T651	<ul style="list-style-type: none"> <li>• Unformed chip thickness, cutting force, temperature, and surface roughness</li> </ul>	<ul style="list-style-type: none"> <li>• Relationship of frequency and amplitude with the machining force, temperature, and the degree of fluctuation</li> </ul>
[154]	Ultrasonic-assisted drilling	Al6061	<ul style="list-style-type: none"> <li>• Thrust force, torque, and surface roughness</li> </ul>	<ul style="list-style-type: none"> <li>• For better thrust force, torque, and surface roughness—low feed rate and high amplitude</li> </ul>
[158]	Water-jet-assisted laser machining	Al7075	<ul style="list-style-type: none"> <li>• Temperature field detection</li> </ul>	<ul style="list-style-type: none"> <li>• Better surface at:</li> <li>• Incident angle: 45°, water jet speed: 14 m/s, laser power: 100 W, laser scanning speed: 1.2 mm/s</li> </ul>

parameters are used then it reduces friction coefficient, thrust force, torque, surface roughness, and thus better quality of machined workpiece. The different work associated with vibration sensors are shown in Table 6.

Further studies into ultraprecision machining were carried out by Khaghani and Cheng [159]. The study presented an innovative approach for analyzing the accuracy and precision of such systems. The study was supported by experimental tests and data on precision machining of contact lens molds. Statistical models were developed to analyze the geometric eccentricity of components before and after precision machining. A maximum standard deviation of 16 nm and a residual of 5 nm in geometric eccentricity were achieved after precision machining of all 26 components of the contact lens mold. The system achieved 76% accuracy and precision with a positioning range of 2–40 nm. The surface finish was also remarkable, with a maximum of 4-nm  $R_a$  and 43-nm PV achieved in the experiments. The study also found that the clamping rigidity of the smart chuck positively impacts the precision of the machining system, suggesting that it could be used as an effective universal device for ultraprecision production purposes. In another study by Özbek et al. [160], the effects of vibration and cutting zone temperature on surface roughness and tool wear during eco-friendly MQL turning of AISI D2 steel were examined. Comparisons were made between dry machining conditions and MQL conditions, evaluating factors such as temperature, cutting tool vibration amplitude, tool wear, surface roughness, and tool life. The results demonstrated that MQL machining outperformed dry machining by reducing cutting tool wear, cutting zone temperature, and cutting tool vibration amplitude. Furthermore, surface roughness improved by 89% and tool life increased by up to 267% with MQL machining compared to dry machining.

## 5 Challenges and future trends

- As the literature shows, aluminum alloys will continue to dominate many industrial applications. According to some reports, the aluminum market will see an annual steady growth ranging from 5.7 to 6.2% in the next decade and is anticipated to reach US\$283 billion by 2032 [161–163]. Their machinability has developed in the past few decades thanks to the introduction of new machining technologies. However, due to the continuous rise in energy prices and high demands for sustainable machining processes, new technologies are now focused on achieving parts machined with minimal energy consumption and cleaner production processes. In this regard, combined machining which is a technology that can conduct multiple machining/manufacturing processes, respectively, in a continue manner [164] can be a viable solution for machining aluminum alloys. Hybrid machining is more suited for metals with low ductility such as aluminum alloys and metals which have high growth in demand.
- Nowadays, additive manufacturing is extensively used in numerous industrial sectors thanks to its ability to produce components with complex geometries and minimal material waste. Additive manufacturing of metals, especially high-strength aluminum alloys, is in high demand due to its excellent mechanical properties and machinability. However, the process is not perfect and many defects such as poor surface finish, porosity, oxidation, and loss of alloying elements during the manufacturing process cannot be completely eliminated [165]. Therefore, machining post-additive manufacturing is gaining a lot of interest among researchers and industries due to its importance in improving the geometry and surface quality of AM components. In

this regard, it is necessary to understand the influence of machining parameters on the residual stresses in AM components especially for the newly added aluminum alloys. This includes understanding the role of tool geometry, coating, cutting parameters, and coolants on the microstructure of the machined surfaces. Previous studies also suggest the implementation of a controlled system which can adjust the cutting force requirements according to the work geometry and build conditions [166]. The studies reported in the open literature on machining AM components made from aluminum alloys are scarce [167–169], and therefore, it is important to understand the implications for machining parameters and strategy on their structural performance such as fatigue [169, 170].

- Smart machining is a process based on real-time process monitoring and intelligent control which can realize decision making of the machining process using machine learning algorithms, to improve part quality, reduce costs, and realize rapid manufacturing as shown in Fig. 22 [171]. The aim is to produce perfectly machined components from the first time. Smart machining requires integrating hardware components and software into new or existing machining systems. However, the process is far from perfect due to the high complexity of the machining process and the lack of robust machining models/algorithms. Since aluminum alloys are somewhat considered to be the easiest to machine compared to other metals and are extensively used in different industries, it is logical to incorporate smart machining and the devel-

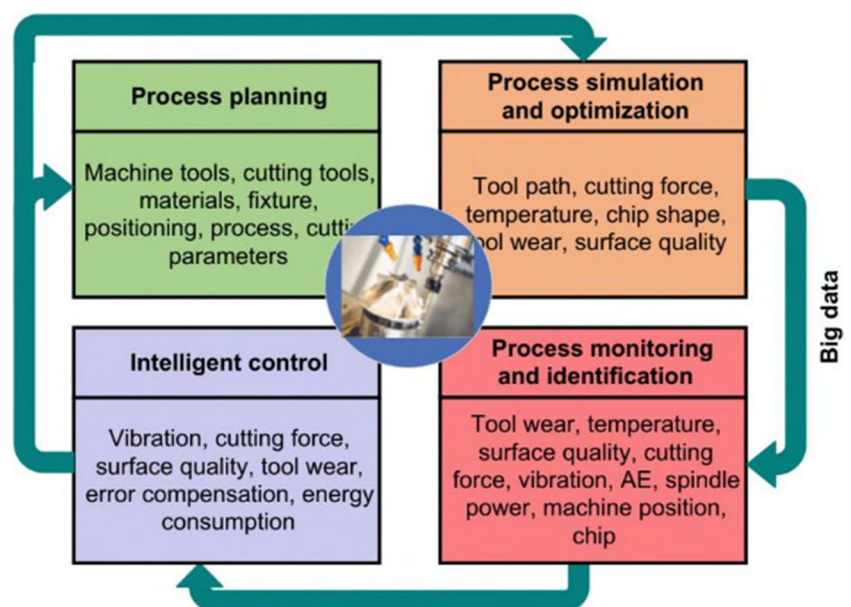
opment of smart machining systems for optimizing their machinability.

## 6 Conclusions

This paper provides a state-of-the-art review on the machinability of aluminum and its alloys. The review focuses on the fundamentals of machining inputs and outputs that govern the quality of aluminum and its alloys. The effects of cutting parameters on surface integrity, tool wear, material removal rate, and chip morphology are discussed and analyzed. Improvements of machining inputs and outputs via different aspects are also discussed and reported including the use of coolants, tool geometry, tool coating, and hybridization of machining processes as a tool to reduce thermal and mechanical forms of damage. Finally, challenges and future trends related to the machining of aluminum and its alloys are summarized. Based on the reviewed literature, the following conclusions can be drawn:

- Tool wear is significantly lower when machining aluminum alloys than when machining other metals such as steel. This observation is explained primarily by the fact that aluminum alloys have lower strength and greater ductility than steel, resulting in tool wear rates that are at least 30–40% lower in similar cutting conditions. Nevertheless, improving surface integrity in aluminum alloys remains critical because it has a direct impact on the structural integrity of machined parts and can have a

**Fig. 22** An example of a smart machining system [171]



significant impact on its corrosion resistance and fatigue life.

- Cutting speed has a significant impact on the microstructural alterations in aluminum alloys that occur after machining. The relationship between rising temperatures — typically between 200 and 400 °C — and faster cutting rates is evident. These temperatures change the characteristics of the machined surface, causing variations in hardness and surface roughness of up to 15% and 20%, respectively.
- The surface integrity and productivity of machined aluminum alloys are significantly influenced by the cutting tool's characteristics (i.e., geometry, coating, tool material). Specific coatings can increase surface finish by up to 25%, extend tool life by up to 30%, and decrease edge formation by up to 40% when compared to coatings that contain aluminum or other elements that typically have a lower chemical affinity with the alloy. Surface integrity and higher material removal rates can both be impacted by tool material; for example, diamond tools perform up to 50% better than high-speed steel tools. The clearance angle in the tool geometry needs to be small enough to prevent weakness at the cutting edge while still preventing friction between the tool and the aluminum workpiece.
- Chip morphology is critical in the machining of aluminum alloys because it affects both surface integrity and productivity. A variety of factors, including cutting parameters, coolant use, geometry, coating, and cutting tool material, influence the intricate phenomenon of chip formation. By adjusting these factors, chip formation can be controlled to improve surface integrity and tool life. Changing the feed rate and cutting speed of cutting mechanisms (ploughing, shearing, and microcutting, for example) can increase tool life by up to 35%.
- It has been proven that using vibration techniques during the machining of aluminum alloys can reduce thermal effects and improve surface finish by up to 40%. When proper frequency and amplitude are used, cutting forces can be reduced by around 30%, which lowers friction and stresses in the cutting zone during machining.

**Data availability** Not applicable.

**Code availability** Not applicable.

## Declarations

**Ethics approval** Not applicable.

**Consent to participate** Not applicable.

**Consent for publication** Not applicable.

**Conflict of interest** The authors declare no competing interests.

**Open Access** This article is licensed under a Creative Commons Attribution 4.0 International License, which permits use, sharing, adaptation, distribution and reproduction in any medium or format, as long as you give appropriate credit to the original author(s) and the source, provide a link to the Creative Commons licence, and indicate if changes were made. The images or other third party material in this article are included in the article's Creative Commons licence, unless indicated otherwise in a credit line to the material. If material is not included in the article's Creative Commons licence and your intended use is not permitted by statutory regulation or exceeds the permitted use, you will need to obtain permission directly from the copyright holder. To view a copy of this licence, visit <http://creativecommons.org/licenses/by/4.0/>.

## References

1. Kui GWA, Islam S, Reddy MM, Khandoker N, Chen VLC (2022) Recent progress and evolution of coolant usages in conventional machining methods: a comprehensive review. *Int J Adv Manuf Technol* 119(1):3–40. <https://doi.org/10.1007/s00170-021-08182-0>
2. Duan Z, Li C, Ding W, Zhang Y, Yang M, Gao T, Cao H, Xu X, Wang D, Mao C, Li HN, Kumar GM, Said Z, Debnath S, Jamil M, Ali HM (2021) Milling force model for aviation aluminum alloy: academic insight and perspective analysis. *Chin J Mech Eng* 34(1):18. <https://doi.org/10.1186/s10033-021-00536-9>
3. Santos MC, Machado AR, Sales WF, Barrozo MAS, Ezugwu EO (2016) Machining of aluminum alloys: a review. *Int J Adv Manuf Technol* 86(9):3067–3080. <https://doi.org/10.1007/s00170-016-8431-9>
4. Syreyschikova NV, Guzeev VI, Ardashev DV, Pimenov DY, Patra K, Kapłonek W, Nadolny K (2020) A study on the machinability of steels and alloys to develop recommendations for setting tool performance characteristics and belt grinding modes. *Materials* 13(18):3978. <https://doi.org/10.3390/ma13183978>
5. Machado AR, Wallbank J (1990) Machining of titanium and its alloys—a review. 204(1):53–60 [https://doi.org/10.1243/pime\\_proc\\_1990\\_204\\_047\\_02](https://doi.org/10.1243/pime_proc_1990_204_047_02)
6. Dey S, Chakraborty S, JSDSL (2016) A study on the machinability of some metal alloys using grey TOPSIS method. 5(1):31–44 <https://doi.org/10.5267/j.dsl.2015.9.002>
7. Bork CAS, Gonçalves JFDS, Gomes JDO, Gheller J (2014) Performance of the jatropa vegetable-base soluble cutting oil as a renewable source in the aluminum alloy 7050–T7451 millin. *CIRP J Manuf Sci Technol* 7(3):210–221. <https://doi.org/10.1016/j.cirpj.2014.04.004>
8. Li J-G, Wang S-Q (2017) Distortion caused by residual stresses in machining aeronautical aluminum alloy parts: recent advances. *Int J Adv Manuf Technol* 89(1):997–1012. <https://doi.org/10.1007/s00170-016-9066-6>
9. Del Sol I, Rivero A, López de Lacalle LN, Gamez AJ (2019) Thin-wall machining of light alloys: a review of models and industrial approaches. *Materials* 12(12):2012. <https://doi.org/10.3390/ma12122012>
10. Aamir M, Giasin K, Tolouei-Rad M, Vafadar A (2020) A review: drilling performance and hole quality of aluminium alloys for aerospace applications. *J Market Res* 9(6):12484–12500. <https://doi.org/10.1016/j.jmrt.2020.09.003>



11. Sarikaya M, Gupta MK, Tomaz I, Danish M, Mia M, Rubaieef S, Jamil M, Pimenov DY, Khanna N (2020) Cooling techniques to improve the machinability and sustainability of light-weight alloys: a state-of-the-art review. *J Manuf Processes* 62:179–201. <https://doi.org/10.1016/j.jmapro.2020.12.013>
12. Vijay R, Aju Kumar VN, Sadiq A, Thomas L (2022) Influence of cryogenic treatment on bulk and surface properties of aluminium alloys: a review. *Adv Mater Process Technol*, 1–12 <https://doi.org/10.1080/2374068X.2022.2072085>
13. Brown T, Idoine N, Wrighton C, Raycraft E, Hobbs S, Shaw R, Everett, P, Deady E, Kresse C (2021) World mineral production 2015–2019
14. Schlesinger ME (2013) Aluminum recycling. CRC press
15. Kvande H, Occurrence and production of aluminum, in *Encyclopedia of Inorganic and Bioinorganic Chemistry*. 1–10. <https://doi.org/10.1002/9781119951438.eibc2350>.
16. Soiński MS, Jakubus A (2021) The leading role of aluminium in the growing production of castings made of the non-ferrous alloys. *Arch Foundry Eng* 21(No 3):33–42. <https://doi.org/10.24425/afe.2021.136110>
17. Institute IA. <https://international-aluminium.org/>. [cited 2023 15/01/2023].
18. Liu G, Müller DB (2012) Addressing sustainability in the aluminum industry: a critical review of life cycle assessments. *J Clean Prod* 35:108–117. <https://doi.org/10.1016/j.jclepro.2012.05.030>
19. Azarniya A, Taheri AK, Taheri KK (2019) Recent advances in ageing of 7xxx series aluminum alloys: a physical metallurgy perspective. *J Alloy Compd* 781:945–983. <https://doi.org/10.1016/j.jallcom.2018.11.286>
20. Rambabu P, Eswara Prasad N, Kutumbarao VV, Wanhill RJH (2017) Aluminium alloys for aerospace applications, in *Aerospace Materials and Material Technologies : Volume 1: Aerospace Materials*, N.E. Prasad and R.J.H. Wanhill, Editors, Springer Singapore: Singapore. p. 29–52. [https://doi.org/10.1007/978-981-10-2134-3\\_2](https://doi.org/10.1007/978-981-10-2134-3_2).
21. Javidani M, Larouche D (2014) Application of cast Al–Si alloys in internal combustion engine components. *Int Mater Rev* 59(3):132–158. <https://doi.org/10.1179/1743280413Y.0000000027>
22. Umezawa O, Nagai K (1999) Microstructural refinement of an as-cast Al–12.6 wt pct Si alloy by repeated thermomechanical treatment to produce a heavily deformable material. *Metall Mater Trans A* 30(8):2221–2228. <https://doi.org/10.1007/s11661-999-0034-8>
23. Ponweiser N, Richter KW (2012) New investigation of phase equilibria in the system Al–Cu–Si. *J Alloy Compd* 512(1):252–263. <https://doi.org/10.1016/j.jallcom.2011.09.076>
24. Pan XM, Lin C, Brody HD, Morral JE (2005) An assessment of thermodynamic data for the liquid phase in the Al-rich corner of the Al–Cu–Si system and its application to the solidification of a 319 alloy. *J Phase Equilib Diffus* 26(3):225–233. <https://doi.org/10.1007/s11669-005-0109-1>
25. Gouveia GL, Gomes LF, Cheung N, Garcia A, Spinelli JE (2021) Mechanical properties, microstructural features, and correlations with solidification rates of Al–Cu–Si ultrafine eutectic alloys. 23(4):2001177. <https://doi.org/10.1002/adem.202001177>
26. Kozana J, Piękoś M, Maj M, Garbacz-Klempka A, Żak PL (2020) Analysis of the microstructure, properties and machinability of Al–Cu–Si alloys. *Arch Foundry Eng* 20(No 4):145–153. <https://doi.org/10.24425/afe.2020.136069>
27. Awe SA (2021) Elevated temperature tensile properties of a ternary eutectic Al–27% Cu–5% Si cast alloy. *Int J Light Mater Manuf* 4(1):18–26. <https://doi.org/10.1016/j.ijlmm.2020.07.004>
28. Awe SA (2021) Solidification and microstructural formation of a ternary eutectic Al–Cu–Si cast alloy. *J King Saud Univ - Eng Sci* 33(8):569–580. <https://doi.org/10.1016/j.jksues.2020.07.004>
29. Balos S, Rajnovic D, Sidjanin L, Savkovic B, Kovac P, Janjatovic P (2019) Tensile and fatigue properties, machinability and machined surface roughness of Al–Si–Cu alloys. *Matéria (Rio de Janeiro)*. 24
30. Polmear I, StJohn D, Nie J-F, Qian M (2017) Light alloys: metallurgy of the light metals.: Butterworth-Heinemann
31. Lee B-H, Kim S-H, Park J-H, Kim H-W, Lee J-C (2016) Role of Mg in simultaneously improving the strength and ductility of Al–Mg alloys. *Mater Sci Eng A* 657:115–122. <https://doi.org/10.1016/j.msea.2016.01.089>
32. Hall EO (1951) The deformation and ageing of mild steel: III Discussion of results. *Proc Phys Soc Sect B* 64(9):747. <https://doi.org/10.1088/0370-1301/64/9/303>
33. Petch NJ (1953) The cleavage strength of polycrystals. *J Iron Steel Res Int* 174:25–28
34. Easton M, Wang H, Grandfield J, St John D, Sweet E (2004) An analysis of the effect of grain refinement on the hot tearing of aluminium alloys. in *Materials forum*
35. StJohn DH, Qian M, Easton MA, Cao P, Hildebrand Z (2005) Grain refinement of magnesium alloys. *Metall Mater Trans A* 36(7):1669–1679. <https://doi.org/10.1007/s11661-005-0030-6>
36. Darling KA, Roberts AJ, Armstrong L, Kapoor D, Tschopp MA, Kecskes LJ, Mathaudhu SN (2014) Influence of Mn solute content on grain size reduction and improved strength in mechanically alloyed Al–Mn alloys. *Mater Sci Eng A* 589:57–65. <https://doi.org/10.1016/j.msea.2013.09.047>
37. Zhu X-H, Lin YC, Wu Q, Jiang Y-Q (2020) Effects of aging on precipitation behavior and mechanical properties of a tensile deformed Al–Cu alloy. *J Alloy Compd* 843:155975. <https://doi.org/10.1016/j.jallcom.2020.155975>
38. Song YF, Ding XF, Zhao XJ, Xiao LR, Guo L (2017) The effect of stress-aging on dimensional stability behavior of Al–Cu–Mg alloy. *J Alloy Compd* 718:298–303. <https://doi.org/10.1016/j.jallcom.2017.05.183>
39. Jang J-H, Nam D-G, Park Y-H, Park I-M (2013) Effect of solution treatment and artificial aging on microstructure and mechanical properties of Al–Cu alloy. *Trans Nonferrous Metals Soc China* 23(3):631–635. [https://doi.org/10.1016/S1003-6326\(13\)62509-1](https://doi.org/10.1016/S1003-6326(13)62509-1)
40. Li J, Lü S, Wu S, Zhao D, Guo W (2022) Micro-mechanism of simultaneous improvement of strength and ductility of squeeze-cast Al–Cu alloy. *Mater Sci Eng A* 833:142538. <https://doi.org/10.1016/j.msea.2021.142538>
41. Dong X, Guo Y, Wang J, Xia F, Ma K, Duan H, Yang Z, Wang P, Liang M, Li J (2023) Novel AlCu solute cluster precipitates in the Al–Cu alloy by elevated aging and the effect on the tensile properties. *Mater Sci Eng A* 862:144454. <https://doi.org/10.1016/j.msea.2022.144454>
42. Samarendra R, Shibayan R (2022) New-age Al–Cu–Mn–Zr (ACMZ) alloy for high temperature-high strength applications: a review, in *Aluminium Alloys*, T. Giulio, Editor, IntechOpen: Rijeka. p. Ch. 2. <https://doi.org/10.5772/intechopen.104533>
43. Heinz A, Haszler A, Keidel C, Moldenhauer S, Benedictus R, Miller WS (2000) Recent development in aluminium alloys for aerospace applications. *Mater Sci Eng A* 280(1):102–107. [https://doi.org/10.1016/S0921-5093\(99\)00674-7](https://doi.org/10.1016/S0921-5093(99)00674-7)
44. Li Z, Chen L, Tang J, Zhao G, Zhang C (2020) Response of mechanical properties and corrosion behavior of Al–Zn–Mg alloy treated by aging and annealing: a comparative study. *J Alloy Compd* 848:156561. <https://doi.org/10.1016/j.jallcom.2020.156561>
45. Shu WX, Hou LG, Zhang C, Zhang F, Liu JC, Liu JT, Zhuang LZ, Zhang JS (2016) Tailored Mg and Cu contents affecting the

- microstructures and mechanical properties of high-strength Al–Zn–Mg–Cu alloys. *Mater Sci Eng A* 657:269–283. <https://doi.org/10.1016/j.msea.2016.01.039>
46. Zou Y, Wu X, Tang S, Zhu Q, Song H, Guo M, Cao L (2021) Investigation on microstructure and mechanical properties of Al–Zn–Mg–Cu alloys with various Zn/Mg ratios. *J Mater Sci Technol* 85:106–117. <https://doi.org/10.1016/j.jmst.2020.12.045>
  47. Gloria A, Montanari R, Richetta M, Varone A (2019) Alloys for aeronautic applications: state of the art and perspectives. 9(6):662
  48. Robson JD, Engler O, Sigli C, Deschamps A, Poole WJ (2020) Advances in microstructural understanding of wrought aluminum alloys. *Metall Mater Trans A* 51(9):4377–4389. <https://doi.org/10.1007/s11661-020-05908-9>
  49. Milagre MX, Franco M, Genezini F, Wimpory RC, Yokaichiya F, Costa I (2020) A correlation between microstructure and residual stress in the 6061 Al–Mg–Si alloy with different thermomechanical process. *SN Appl Sci* 2(12):2106. <https://doi.org/10.1007/s42452-020-03945-y>
  50. Froehlich AR, Jacques RC, Strohaecker TR, Mombru RJJOME, Performance (2007) The correlation of machinability and microstructural characteristics of different extruded aluminum alloys 16:784–791. <https://doi.org/10.1007/S11665-007-9097-0>
  51. Horváth R, Drégelyi-Kiss Á (2015) Analysis of surface roughness of aluminum alloys fine turned: united phenomenological models and multi-performance optimization. *Measurement* 65:181–192. <https://doi.org/10.1016/j.measurement.2015.01.013>
  52. Xu J, Li L, Lin T, Gupta MK, Chen M (2022) Machinability analysis in high-speed milling of AlSi7Mg alloys under EMQL conditions: an approach toward sustainable manufacturing. *J Manuf Process* 81:1005–1017. <https://doi.org/10.1016/j.jmapro.2022.07.010>
  53. Yücel A, Yıldırım ÇV, Sankaya M, Şirin Ş, Kivak T, Gupta MK, Tomaz ÍV (2021) Influence of MoS<sub>2</sub> based nanofluid-MQL on tribological and machining characteristics in turning of AA 2024 T3 aluminum alloy. *J Market Res* 15:1688–1704. <https://doi.org/10.1016/j.jmrt.2021.09.007>
  54. Zhang P, Zhang X, Cao X, Yu X, Wang Y (2021) Analysis on the tool wear behavior of 7050–T7451 aluminum alloy under ultrasonic elliptical vibration cutting. *Wear* 466–467:203538. <https://doi.org/10.1016/j.wear.2020.203538>
  55. Nouri H, Farahnakian M, Elhami S (2017) Experimental study on the wettability of microtextured surfaces generated by the ultrasonic-assisted face turning. 231(5):655–663. <https://doi.org/10.1177/1350650116672144>
  56. Khanali M, Farahnakian M, Elhami S, Khani S (2022) Tribological properties of vibro-mechanical texturing during face turning processes. *Int J Light Mater Manuf* 5(1):91–101. <https://doi.org/10.1016/j.ijlmm.2021.11.001>
  57. Chongyang Z, Junyu L, Xiaobo W, Bo Z (2022) Wettability of high-performance aluminum alloy surfaces machined longitudinal-torsion ultrasonic-assisted milling. *China Mech Eng* 33(16). <https://doi.org/10.3969/J.ISSN.1004-132X.2022.16.004>
  58. Zamani M, Farahnakian M, Elhami S (2021) Employment of ultrasonic assisted turning in the fabrication of microtextures to improve the surface adhesion of the titanium implant. 235(12):1983–1991. <https://doi.org/10.1177/09544054211011029>
  59. Ni H, Elmadagli M, Alpas AT (2004) Mechanical properties and microstructures of 1100 aluminum subjected to dry machining. *Mater Sci Eng A* 385(1):267–278. <https://doi.org/10.1016/j.msea.2004.06.048>
  60. Rotella G (2019) Effect of surface integrity induced by machining on high cycle fatigue life of 7075–T6 aluminum alloy. *J Manuf Process* 41:83–91. <https://doi.org/10.1016/j.jmapro.2019.03.031>
  61. Wang B, Liu Z (2016) Investigations on deformation and fracture behavior of workpiece material during high speed machining of 7050–T7451 aluminum alloy. *CIRP J Manuf Sci Technol* 1443–54. <https://doi.org/10.1016/j.cirpj.2016.05.007>
  62. Fergani O, Shao Y, Liang SY (2014) Effect of temperature on the subsurface microstructure and mechanical properties of AA 7075–T6 in machining. *Procedia CIRP* 13:181–185. <https://doi.org/10.1016/j.procir.2014.04.031>
  63. Liu H, Guo Y, Du Y (2022) The removal mechanism transformation from crystalline to amorphous in nano-machining Cu–Al alloy. *Mater Today Commun* 31:103523. <https://doi.org/10.1016/j.mtcomm.2022.103523>
  64. Cozzens DA II, Rao PD, Olson WW, Sutherland JW, Panetta JM (1999) An experimental investigation into the effect of cutting fluid conditions on the boring of aluminum alloys. *J Manuf Sci Eng* 121(3):434–439. <https://doi.org/10.1115/1.2832700>
  65. Imbrogno S, Rotella G, Rinaldi S (2020) Surface and subsurface modifications of AA7075–T6 induced by dry and cryogenic high speed machining. *Int J Adv Manuf Technol* 107(1):905–918. <https://doi.org/10.1007/s00170-020-05108-0>
  66. Campbell CE, Bendersky LA, Boettinger WJ, Ivester R (2006) Microstructural characterization of Al–7075–T651 chips and work pieces produced by high-speed machining. *Mater Sci Eng A* 430(1):15–26. <https://doi.org/10.1016/j.msea.2006.04.122>
  67. Rotella G, Dillon OW, Umbrello D, Settineri L, Jawahir IS (2013) Finite element modeling of microstructural changes in turning of AA7075–T651 alloy. *J Manuf Process* 15(1):87–95. <https://doi.org/10.1016/j.jmapro.2012.09.005>
  68. Shankar MR, Chandrasekar S, Compton WD, King AH (2005) Characteristics of aluminum 6061–T6 deformed to large plastic strains by machining. *Mater Sci Eng A* 410–411:364–368. <https://doi.org/10.1016/j.msea.2005.08.137>
  69. Guru PR, Khan Md F, Panigrahi SK, Ram GDJ (2015) Enhancing strength, ductility and machinability of a Al–Si cast alloy by friction stir processing. *J Manuf Process* 18:67–74. <https://doi.org/10.1016/j.jmapro.2015.01.005>
  70. Skiba J, Kossakowska J, Kulczyk M, Pachla W, Przybysz S, Smalc-Koziorowska J, Przybysz M (2020) The impact of severe plastic deformations obtained by hydrostatic extrusion on the machinability of ultrafine-grained AA5083 alloy. *J Manuf Process* 58:1232–1240. <https://doi.org/10.1016/j.jmapro.2020.09.023>
  71. Gonçalves RA, Silva MBD (2015) Influence of copper content on 6351 aluminum alloy machinability. *Procedia Manuf* 1:683–695. <https://doi.org/10.1016/j.promfg.2015.09.014>
  72. Soori M, Arezoo B (2022) A review in machining-induced residual stress. *J New Technol Mater* 12:64–83. <https://hal.science/hal-03679993>
  73. Tang ZT, Liu ZQ, Pan YZ, Wan Y, Ai X (2009) The influence of tool flank wear on residual stresses induced by milling aluminum alloy. *J Mater Process Technol* 209(9):4502–4508. <https://doi.org/10.1016/j.jmatprotec.2008.10.034>
  74. Berry L, Wheatley G, Ma W, MasoudiNejad R, Berto F (2022) The influence of milling induced residual stress on fatigue life of aluminum alloys. *Forces Mech* 7:100096. <https://doi.org/10.1016/j.finmec.2022.100096>
  75. Xue N-P, Wu Q, Yang R-S, Gao H-J, Zhang Z, Zhang Y-D, Li L, Guo J (2023) Research on machining deformation of aluminum alloy rolled ring induced by residual stress. *Int J Adv Manuf Technol* 125(11):5669–5680. <https://doi.org/10.1007/s00170-023-11068-y>
  76. Weber D, Kirsch B, Chighizola CR, D’Elia CR, Linke BS, Hill MR, Aurich JC (2021) Analysis of machining-induced residual stresses of milled aluminum workpieces, their repeatability, and their resulting distortion. *Int J Adv Manuf Technol* 115(4):1089–1110. <https://doi.org/10.1007/s00170-021-07171-7>
  77. Li Y, Li Y-N, Li X-W, Zhu K, Zhang Y-A, Li Z-H, Yan H-W, Wen K (2023) Influence of material removal strategy on machining

- deformation of aluminum plates with asymmetric residual stresses. 16(5):2033
78. Rossmann A (2023) Aeroengine safety: Institute of Thermal Turbomachinery and Machine Dynamics. [cited 2023 15/10/2023]; Available from: <https://aeroenginesafety.tugraz.at/doku.php?id=start>
  79. Mathews R, Sunny S, Malik A, Halley J (2022) Coupling between inherent and machining-induced residual stresses in aluminum components. *Int J Mech Sci* 213:106865. <https://doi.org/10.1016/j.ijmecsci.2021.106865>
  80. Denkena B, Boehnke D, de León L (2008) Machining induced residual stress in structural aluminum parts. *Prod Eng Res Devel* 2(3):247–253. <https://doi.org/10.1007/s11740-008-0097-1>
  81. Singh A, Agrawal A (2015) Investigation of surface residual stress distribution in deformation machining process for aluminum alloy. *J Mater Process Technol* 225:195–202. <https://doi.org/10.1016/j.jmatprotec.2015.05.025>
  82. Casuso M, Polvorosa R, Veiga F, Suárez A, Lamikiz A (2020) Residual stress and distortion modeling on aeronautical aluminum alloy parts for machining sequence optimization. *Int J Adv Manuf Technol* 110(5):1219–1232. <https://doi.org/10.1007/s00170-020-05816-7>
  83. Fuh K-H, Wu C-F (1995) A residual-stress model for the milling of aluminum alloy (2014–T6). *J Mater Process Technol* 51(1):87–105. [https://doi.org/10.1016/0924-0136\(94\)01355-5](https://doi.org/10.1016/0924-0136(94)01355-5)
  84. Özbek O, Özbek NA, Kara F, Saruhan H (2023) Effect of vibration and cutting zone temperature on surface topography during hybrid cooling/lubrication assisted machining of Vanadis 10. 65(9):1437–1452. <https://doi.org/10.1515/mt-2023-0057>
  85. Liu B (2015) The impact of machining on the corrosion performance of AA7150-T651 aluminium alloy. The University of Manchester (United Kingdom), Available from: [https://pure.manchester.ac.uk/ws/portalfiles/portal/63039158/FULL\\_TEXT.PDF](https://pure.manchester.ac.uk/ws/portalfiles/portal/63039158/FULL_TEXT.PDF)
  86. Davis JR (2001) Surface engineering for corrosion and wear resistance. ASM international
  87. Liu B, Zhang X, Zhou X, Hashimoto T, Wang J (2017) The corrosion behaviour of machined AA7150-T651 aluminium alloy. *Corros Sci* 126:265–271. <https://doi.org/10.1016/j.corsci.2017.07.008>
  88. Liu B, Zhou XR (2014) The impact of machining on the corrosion behaviour of AA7150-T651 aluminium alloy. *Mater Sci Forum* 794–796:217–222. <https://doi.org/10.4028/www.scientific.net/MSF.794-796.217>
  89. Pei H-J, Chen L-F, Chen S-F, Wang G-C. Corrosion resistance of 7075 aluminum alloy surface by dry turning and MQL machining, in *Materials Science and Engineering*. 537–544 [https://doi.org/10.1142/9789813226517\\_0078](https://doi.org/10.1142/9789813226517_0078)
  90. Fu X, Meng Y, Liu W (2016) Corrosion evaluation of machined surface in aviation aluminum alloy under simulated service environment. in 2016 4th International Conference on Advanced Materials and Information Technology Processing (AMITP 2016). Atlantis Press <https://doi.org/10.2991/amitp-16.2016.31>
  91. Sayadi D, Mahdikhani F, Khajehzadeh M, Khosrojerdi M, Razfar MR, Corrosion resistance improvement of 6061 aluminum alloy by 2D ultrasonic vibrations assisted turning. 0(0):09544062231181807. <https://doi.org/10.1177/09544062231181807>
  92. Sayadi D, Bagheri M, Khosrojerdi M, Khajehzadeh M, Razfar MR (2023) The influence of vibration amplitude on AA7075-T6 corrosion resistance improvement during ultrasonic-assisted burr-removal. 237(9):1990–2008. <https://doi.org/10.1177/14644207231167547>
  93. Nouari M, List G, Girot F, Coupard D (2003) Experimental analysis and optimisation of tool wear in dry machining of aluminium alloys. *Wear* 255(7):1359–1368. [https://doi.org/10.1016/S0043-1648\(03\)00105-4](https://doi.org/10.1016/S0043-1648(03)00105-4)
  94. Lane BM, Shi M, Dow TA, Scattergood R (2010) Diamond tool wear when machining Al6061 and 1215 steel. *Wear* 268(11):1434–1441. <https://doi.org/10.1016/j.wear.2010.02.019>
  95. Musavi SH, Sepehri M, Davoodi B, Niknam SA (2022) Performance analysis of developed micro-textured cutting tool in machining aluminum alloy 7075-T6: assessment of tool wear and surface roughness. *Int J Adv Manuf Technol* 119(5):3343–3362. <https://doi.org/10.1007/s00170-021-08349-9>
  96. Liu J, Kevin Chou Y (2007) On temperatures and tool wear in machining hypereutectic Al–Si alloys with vortex-tube cooling. *Int J Mach Tools Manuf* 47(3):635–645. <https://doi.org/10.1016/j.ijmactools.2006.04.008>
  97. Abas M, Sayd L, Akhtar R, Khalid QS, Khan AM, Pruncu CI (2020) Optimization of machining parameters of aluminum alloy 6026–T9 under MQL-assisted turning process. *J Market Res* 9(5):10916–10940. <https://doi.org/10.1016/j.jmrt.2020.07.071>
  98. Rathod P, Aravindan S, Venkateswara Rao P (2016) Performance evaluation of novel micro-textured tools in improving the machinability of aluminum alloy (Al 6063). *Procedia Technol* 23:296–303. <https://doi.org/10.1016/j.protcy.2016.03.030>
  99. Bansal P, Upadhyay L (2016) Effect of turning parameters on tool wear, surface roughness and metal removal rate of alumina reinforced aluminum composite. *Procedia Technol* 23:304–310. <https://doi.org/10.1016/j.protcy.2016.03.031>
  100. Manjunath Patel GC, Lokare D, Chate GR, Parappagoudar MB, Nikhil R, Gupta K (2020) Analysis and optimization of surface quality while machining high strength aluminium alloy. *Measurement* 152:107337. <https://doi.org/10.1016/j.measurement.2019.107337>
  101. Barzani MM, Sarhan AAD, Farahany S, Ramesh S, Maher I (2015) Investigating the machinability of Al–Si–Cu cast alloy containing bismuth and antimony using coated carbide insert. *Measurement* 62:170–178. <https://doi.org/10.1016/j.measurement.2014.10.030>
  102. Xu K, Zou B, Wang Y, Guo P, Huang C, Wang J (2016) An experimental investigation of micro-machinability of aluminum alloy 2024 using Ti(C7N3)-based cermet micro end-mill tools. *J Mater Process Technol* 235:13–27. <https://doi.org/10.1016/j.jmatprotec.2016.04.011>
  103. Wang B, Liu Z (2017) Acoustic emission signal analysis during chip formation process in high speed machining of 7050–T7451 aluminum alloy and Inconel 718 superalloy. *J Manuf Process* 27:114–125. <https://doi.org/10.1016/j.jmapro.2017.04.003>
  104. Eapen J, Murugappan S, Arul S (2017) A study on chip morphology of aluminum alloy 6063 during turning under pre cooled cryogenic and dry environments. *Mater Today Proc* 4(8):7686–7693. <https://doi.org/10.1016/j.matpr.2017.07.103>
  105. Davis JR (1993) Aluminum and aluminum alloys. ASM international <https://doi.org/10.1361/autb2001p351>
  106. Taylor JA (2004) The effect of iron in Al-Si casting alloys. in 35th Australian foundry institute national conference, Adelaide, South Australia
  107. Tanaka T, Akasawa T (1999) Machinability of hypereutectic silicon-aluminum alloys. *J Mater Eng Perform* 8(4):463–468. <https://doi.org/10.1361/105994999770346774>
  108. Wain N, Thomas NR, Hickman S, Wallbank J, Teer DG (2005) Performance of low-friction coatings in the dry drilling of automotive Al–Si alloys. *Surf Coat Technol* 200(5):1885–1892. <https://doi.org/10.1016/j.surfcoat.2005.08.016>
  109. Hovsepian PE, Luo Q, Robinson G, Pittman M, Howarth M, Doerwald D, Tietema R, Sim WM, Deeming A, Zeus T (2006) TiAlN/VN superlattice structured PVD coatings: a new alternative in machining of aluminium alloys for aerospace and automotive components. *Surf Coat Technol* 201(1):265–272. <https://doi.org/10.1016/j.surfcoat.2005.11.106>



110. Narahari P, Pai BC, Pillai RM (1999) Some aspects of machining cast Al-SiCp composites with conventional high speed steel and tungsten carbide tools. *J Mater Eng Perform* 8(5):538–542. <https://doi.org/10.1007/s11665-999-0006-6>
111. Wang B, Liu Z, Song Q, Wan Y, Shi Z (2016) Proper selection of cutting parameters and cutting tool angle to lower the specific cutting energy during high speed machining of 7050–T7451 aluminum alloy. *J Clean Prod* 129:292–304. <https://doi.org/10.1016/j.jclepro.2016.04.071>
112. Carrilero MS, Marcos M (1996) On the machinability of aluminium and aluminium alloys 7(3):179–194. <https://doi.org/10.1515/JMBM.1996.7.3.179>
113. Revel P, Khanfir H, Fillit R-Y (2006) Surface characterization of aluminum alloys after diamond turning. *J Mater Process Technol* 178(1):154–161. <https://doi.org/10.1016/j.jmatprotec.2006.03.169>
114. Unnikrishna Pillai J, Sanghrajka I, Shunmugavel M, Muthuralingam T, Goldberg M, Littlefair G (2018) Optimisation of multiple response characteristics on end milling of aluminium alloy using Taguchi-Grey relational approach. *Measurement* 124:291–298. <https://doi.org/10.1016/j.measurement.2018.04.052>
115. Agustina de B, Saa A, Marcos Bárcena M, Rubio EM (2011) Analysis of the machinability of aluminium alloys UNS A97050–T7 and UNS A92024–T3 during short dry turning tests. *Adv Mater Res* 264–265:931–936. <https://doi.org/10.4028/www.scientific.net/AMR.264-265.931>
116. Bhushan RK (2013) Optimization of cutting parameters for minimizing power consumption and maximizing tool life during machining of Al alloy SiC particle composites. *J Clean Prod* 39:242–254. <https://doi.org/10.1016/j.jclepro.2012.08.008>
117. Bhushan RK (2013) Multiresponse optimization of Al alloy-SiC composite machining parameters for minimum tool wear and maximum metal removal rate. *J Manuf Sci Eng* 135(2). <https://doi.org/10.1115/1.4023454>
118. Puvanesan M, Rahman M, Najiha M, Kadirgama K (2014) Experimental investigation of minimum quantity lubrication on tool wear in aluminum alloy 6061–t6 using different cutting tools. *Int J Automot Mech Eng*. <https://doi.org/10.15282/ijame.9.2013.5.0127>
119. Yousefi R, Ichida Y (2000) A study on ultra-high-speed cutting of aluminium alloy: formation of welded metal on the secondary cutting edge of the tool and its effects on the quality of finished surface. *Precis Eng* 24(4):371–376. [https://doi.org/10.1016/S0141-6359\(00\)00048-9](https://doi.org/10.1016/S0141-6359(00)00048-9)
120. Abbas AT, Pimenov DY, Erdakov IN, Taha MA, El Rayes MM, Soliman MS (2018) Artificial intelligence monitoring of hardening methods and cutting conditions and their effects on surface roughness, performance, and finish turning costs of solid-state recycled aluminum alloy 6061 chips. 8(6):394
121. Chuchala D, Dobrzynski M, Pimenov DY, Orłowski KA, Krolczyk G, Giasin K (2021) Surface roughness evaluation in thin EN AW-6086-T6 alloy plates after face milling process with different strategies. *Materials (Basel)* 14(11). <https://doi.org/10.3390/ma14113036>
122. Singh PK (2021) Optimization of machining parameters for turning of aluminium alloy-2011 using Taguchi method. in IOP Conference Series: Materials Science and Engineering. IOP Publ <https://doi.org/10.1088/1757-899X/1116/1/012092>
123. Liew WYH, Hutchings IM, Williams JA (1998) Friction and lubrication effects in the machining of aluminium alloys. *Tribol Lett* 5(1):117–122. <https://doi.org/10.1023/A:1019164918708>
124. Liew WYH, Hutchings IM, Williams JA (1999) The interaction between tool material, environment, and process conditions in the machining of aluminium alloys. *Mach Sci Technol* 3(2):273–286. <https://doi.org/10.1080/10940349908945694>
125. Wang Z, Kovvuri V, Araujo A, Bacci M, Hung WNP, Bukkapatnam STS (2016) Built-up-edge effects on surface deterioration in micromilling processes. *J Manuf Process* 24:321–327. <https://doi.org/10.1016/j.jmapro.2016.03.016>
126. Sreejith PS, Ngoi BKA (2000) Dry machining: machining of the future. *J Mater Process Technol* 101(1):287–291. [https://doi.org/10.1016/S0924-0136\(00\)00445-3](https://doi.org/10.1016/S0924-0136(00)00445-3)
127. Mendes OC, Ávila RF, Abrão AM, Reis P, Paulo Davim J (2006) The performance of cutting fluids when machining aluminium alloys. *Ind Lubr Tribol* 58(5):260–268. <https://doi.org/10.1108/00368790610682662>
128. Cetin MH, Kabavekilincarslan S (2020) Effects of cutting fluids with nano-silver and borax additives on milling performance of aluminium alloys. *J Manuf Process* 50:170–182. <https://doi.org/10.1016/j.jmapro.2019.12.042>
129. Rivero A, Aramendi G, Herranz S, López de Lacalle LN (2006) An experimental investigation of the effect of coatings and cutting parameters on the dry drilling performance of aluminium alloys. *Int J Adv Manuf Technol* 28(1):1–11. <https://doi.org/10.1007/s00170-004-2349-3>
130. Dhar NR, Islam MW, Islam S, Mithu MAH (2006) The influence of minimum quantity of lubrication (MQL) on cutting temperature, chip and dimensional accuracy in turning AISI-1040 steel. *J Mater Process Technol* 171(1):93–99. <https://doi.org/10.1016/j.jmatprotec.2005.06.047>
131. Sreejith PS (2008) Machining of 6061 aluminium alloy with MQL, dry and flooded lubricant conditions. *Mater Lett* 62(2):276–278. <https://doi.org/10.1016/j.matlet.2007.05.019>
132. Batista Ponce M, Del Sol Illana I, Fernandez-Vidal SR, Salguero Gomez J (2018) Experimental parametric model for adhesion wear measurements in the dry turning of an AA2024 alloy. *Materials* 11(9):1598. <https://doi.org/10.3390/ma11091598>
133. Niknam SA, Jalali A (2020) Effects of lubricants and flow rates on the surface roughness and chip thickness when MQL turning of aero-engine aluminum alloys 6061–T6 and 7076–T6. *Int J Adv Manuf Technol* 110(7):2015–2022. <https://doi.org/10.1007/s00170-020-05979-3>
134. Gupta MK, Mia M, Singh G, Pimenov DY, Sarikaya M, Sharma VS (2019) Hybrid cooling-lubrication strategies to improve surface topography and tool wear in sustainable turning of Al 7075–T6 alloy. *Int J Adv Manuf Technol* 101(1):55–69. <https://doi.org/10.1007/s00170-018-2870-4>
135. Hong SY, Zhao Z (1999) Thermal aspects, material considerations and cooling strategies in cryogenic machining. *Clean Prod Process* 1(2):107–116. <https://doi.org/10.1007/s100980050016>
136. Dobrotă D, Racz S-G, Oleksik M, Rotaru I, Tomescu M, Simion CM, (2022) Smart cutting tools used in the processing of aluminum alloys. 22(1):28
137. Kalyan C, Samuel GL (2015) Cutting mode analysis in high speed finish turning of AlMgSi alloy using edge chamfered PCD tools. *J Mater Process Technol* 216:146–159. <https://doi.org/10.1016/j.jmatprotec.2014.09.003>
138. Songmene V, Khettabi R, Zaghbani I, Kouam J, Djebara AJAATA (2011) Machining and machinability of aluminum alloys. 377:400
139. Brinksmeier E, Janssen R (2002) Drilling of multi-layer composite materials consisting of carbon fiber reinforced plastics (CFRP). *Titanium Alloys CIRR Ann* 51(1):87–90. [https://doi.org/10.1016/S0007-8506\(07\)61472-3](https://doi.org/10.1016/S0007-8506(07)61472-3)
140. Obikawa T, Kamio A, Takaoka H, Osada A (2011) Micro-texture at the coated tool face for high performance cutting. *Int J Mach Tools Manuf* 51(12):966–972. <https://doi.org/10.1016/j.ijmactools.2011.08.013>
141. Dheeraj N, Sanjay S, Kiran Bhargav K, Jagadesh T (2020) Investigations into solid lubricant filled textured tools on hole geometry and surface integrity during drilling of aluminium alloy. *Mater*



- Today Proc 26:991–997. <https://doi.org/10.1016/j.matpr.2020.01.163>
142. Sugihara T, Singh P, Enomoto T (2017) Development of novel cutting tools with dimple textured surfaces for dry machining of aluminum alloys. *Procedia Manuf* 14:111–117. <https://doi.org/10.1016/j.promfg.2017.11.013>
  143. Al-Tameemi HA, Al-Dulaimi T, Awe MO, Sharma S, Pimenov DY, Koklu U, Giasin K (2021) Evaluation of cutting-tool coating on the surface roughness and hole dimensional tolerances during drilling of Al6061-T651 alloy. 14(7):1783
  144. Jasinevicius RG, Otoboni JA, Basso I, Dib MHM (2021) Size effects in ultraprecision machining of aluminum alloys: conventional AA6061-T6 and RSA 6061-T6. *J Manuf Process* 68:136–157. <https://doi.org/10.1016/j.jmapro.2021.07.027>
  145. Khani S, Razfar MR, Haghighi SS, Farahnakian M (2020) Optimization of microtextured tools parameters in thread turning process of aluminum 7075 aerospace alloy. *Mater Manuf Process* 35(12):1330–1338. <https://doi.org/10.1080/10426914.2020.1772485>
  146. Khani S, Shahabi Haghighi S, Razfar MR, Farahnakian M (2021) Improvement of thread turning process using micro-hole textured solid-lubricant embedded tools 235(11):1727–1738. <https://doi.org/10.1177/09544054211019929>
  147. Hoghoughi MH, Farahnakian M, Elhami S (2022) Environmental, economical, and machinability based sustainability assessment in hybrid machining process employing tool textures and solid lubricant. *Sustain Mater Technol* 34:e00511. <https://doi.org/10.1016/j.susmat.2022.e00511>
  148. Haddadzade M, Razfar M, Farahnakian M (2009) Integrating process planning and scheduling for prismatic parts regard to due date. *Int J Ind Manuf Eng* 3(3):248–251. <https://doi.org/10.5281/ZENODO.1330429>
  149. Oles EJ, Inspektor A, Bauer CE (1996) The new diamond-coated carbide cutting tools. *Diam Relat Mater* 5(6):617–624. [https://doi.org/10.1016/0925-9635\(95\)00347-9](https://doi.org/10.1016/0925-9635(95)00347-9)
  150. Fukui H, Okida J, Omori N, Moriguchi H, Tsuda K (2004) Cutting performance of DLC coated tools in dry machining aluminum alloys. *Surf Coat Technol* 187(1):70–76. <https://doi.org/10.1016/j.surfcoat.2004.01.014>
  151. Coldwell HL, Dewes RC, Aspinwall DK, Renevier NM, Teer DG (2004) The use of soft/lubricating coatings when dry drilling BS L168 aluminium alloy. *Surf Coat Technol* 177–178:716–726. <https://doi.org/10.1016/j.surfcoat.2003.08.012>
  152. Yoshikawa H, Nishiyama A (1999) CVD diamond coated insert for machining high silicon aluminum alloys. *Diam Relat Mater* 8(8):1527–1530. [https://doi.org/10.1016/S0925-9635\(99\)00078-3](https://doi.org/10.1016/S0925-9635(99)00078-3)
  153. Bhowmick S, Lukitsch MJ, Alpas AT (2010) Tapping of Al–Si alloys with diamond-like carbon coated tools and minimum quantity lubrication. *J Mater Process Technol* 210(15):2142–2153. <https://doi.org/10.1016/j.jmatprotec.2010.07.032>
  154. Moghaddas MA (2021) Modeling and optimization of thrust force, torque, and surface roughness in ultrasonic-assisted drilling using surface response methodology. *Int J Adv Manuf Technol* 112(9):2909–2923. <https://doi.org/10.1007/s00170-020-06380-w>
  155. Huang HF, Lu D, Wu YB, Yang MM (2012) Finite element analysis of ultrasonic vibration assisted milling of Ti-6Al-4V. in *Advanced Materials Research*. Trans Tech Publ <https://doi.org/10.4028/www.scientific.net/AMR.538-541.823>
  156. Zhao C, Wang X, Zhao B, Jiao F (2018) Microstructure of high-performance aluminum alloy surface processed by the single-excitation same-frequency longitudinal–torsional coupled ultrasonic vibration milling 11(10):1975
  157. Guo M, Wang J, Guo W, Liu J, Jiang X (2022) An unformed chip thickness approach to study the influence of process vibration on machining performance in milling. *Int J Adv Manuf Technol* 120(7):5363–5375. <https://doi.org/10.1007/s00170-022-09088-1>
  158. Chen X, Xu X, Liu W, Huang L, Li H, Wu C, Mu W, Li X (2020) Study on the influence of surface temperature field of aluminum alloy etched by laser water jet composite machining. 13(14):3206
  159. Khaghani A, Cheng K (2020) Investigation on an innovative approach for clamping contact lens mould inserts in ultraprecision machining using an adaptive precision chuck and its application perspectives. *Int J Adv Manuf Technol* 111(3):839–850. <https://doi.org/10.1007/s00170-020-05990-8>
  160. Özbek O, Saruhan H (2020) The effect of vibration and cutting zone temperature on surface roughness and tool wear in eco-friendly MQL turning of AISI D2. *J Market Res* 9(3):2762–2772. <https://doi.org/10.1016/j.jmrt.2020.01.010>
  161. Research AM [26/10/2022]; Available from: <https://www.alliedmarketresearch.com/aluminium-market>
  162. Newswire G (2022) Aluminum market to expand at a 6.2% value CAGR during forecast period 2022–2032. Available from: <https://www.globenewswire.com/en/news-release/2022/08/22/2502091/0/en/Aluminum-Market-to-expand-at-a-6-2-value-CAGR-during-forecast-period-2022-2032-Future-Market-Insights-Inc.html>
  163. Insight FB. The global aluminium market size was \$164.23 billion in 2019 & is projected to reach \$242.44 billion by 2027, at a CAGR of 5.7% during the forecast period.[26/10/2022]; Available from: <https://www.fortunebusinessinsights.com/industry-reports/aluminium-market-100233>.
  164. Dovzhenko N, Sidelnikov S, Dovzhenko I, Galiev R (2017) New technology of combined machining of aluminium alloys. in *Key Engineering Materials*. Trans Tech Publ. <https://doi.org/10.4028/www.scientific.net/KEM.746.29>
  165. Altıparmak SC, Yardley VA, Shi Z, Lin J (2021) Challenges in additive manufacturing of high-strength aluminium alloys and current developments in hybrid additive manufacturing. *Int J Light Mater Manuf* 4(2):246–261. <https://doi.org/10.1016/j.ijlmm.2020.12.004>
  166. Oyelola O, Crawforth P, M'Saoubi R, Clare AT (2016) Machining of additively manufactured parts: implications for surface integrity. *Procedia CIRP* 45:119–122. <https://doi.org/10.1016/j.procir.2016.02.066>
  167. Struzikiewicz G, Sioma A (2022) Surface topographic features after milling of additively manufactured AlSi10Mg aluminum alloy. 15(10):3604
  168. Aldwell B, Kelly E, Wall R, Amaldi A, O'Donnell GE, Lupoi R (2017) Machinability of Al 6061 deposited with cold spray additive manufacturing. *J Therm Spray Technol* 26(7):1573–1584. <https://doi.org/10.1007/s11666-017-0586-x>
  169. Aboulkhair NT, Maskery I, Tuck C, Ashcroft I, Everitt NM (2016) Improving the fatigue behaviour of a selectively laser melted aluminium alloy: influence of heat treatment and surface quality. *Mater Des* 104:174–182. <https://doi.org/10.1016/j.matdes.2016.05.041>
  170. Rao JH, Zhang K, Rometsch P, Huang A, Wu X (2018) The influence of surface roughness on the fatigue performance of selective laser melted aluminium alloy A357. in *Proceedings of the 16th International Aluminium Alloys Conference (ICAA16)*
  171. Zhu K (2021) *Smart machining systems: modelling, monitoring and informatics*. Springer Nat. <https://doi.org/10.1007/978-3-030-87878-8>